Sensitivity of Dynamical Intraseasonal Prediction Skills to Different Initial Conditions*

XIOUHUA FU

IPRC, SOEST, University of Hawaii at Manoa, Honolulu, Hawaii

BIN WANG

IPRC, SOEST, and Department of Meteorology, University of Hawaii at Manoa, Honolulu, Hawaii

JUNE-YI LEE

IPRC, SOEST, University of Hawaii at Manoa, Honolulu, Hawaii

WANQIU WANG

NCEP/CPC, Camp Springs, Maryland

LI GAO

IPRC, SOEST, University of Hawaii at Manoa, Honolulu, Hawaii, and National Meteorological Center, China Meteorological Administration, Beijing, China

(Manuscript received 3 August 2010, in final form 23 February 2011)

ABSTRACT

Predictability of intraseasonal oscillation (ISO) relies on both initial conditions and lower boundary conditions (or atmosphere–ocean interaction). The atmospheric reanalysis datasets are commonly used as initial conditions. Here, the biases of three reanalysis datasets [the NCEP reanalysis 1 and 2 (NCEP-R1 and -R2) and the ECMWF Re-Analysis Interim (ERA-Interim)] in describing ISO were briefly revealed and the impacts of these biases as initial conditions on ISO prediction skills were assessed. A signal-recovery method is proposed to improve ISO prediction.

Although all three reanalyses underestimate the intensity of the equatorial eastward-propagating ISO, the overall quality of the ERA-Interim is better than the NCEP-R1 and -R2. When these reanalyses are used as initial conditions in the ECHAM4-University of Hawaii hybrid coupled model (UH-HCM), skillful ISO prediction reaches only about 1 week for both the 850-hPa zonal winds (U850) and rainfall over Southeast Asia and the global tropics. An enhanced nudging of the divergence field is shown to significantly improve the initial conditions, resulting in an extension of the skillful rainfall prediction by 2–4 days and U850 prediction by 5–10 days.

After recovering the ISO signals in the original reanalyses, the resultant initial conditions contain ISO strength closer to the observed, whereas the rainfall spatial pattern correlation in the ERA-Interim reanalysis drops. The resultant ISO prediction skills, however, are consistently extended for all the NCEP and ERA-Interim reanalyses. Using these signal-recovered reanalyses as initial conditions, the boreal summer ISO prediction skill measured with the Wheeler–Hendon index reaches 14 days. The U850 and rainfall prediction skills, respectively, reach 23 and 18 days over Southeast Asia. It is also found that small-scale synoptic weather disturbances in initial conditions generally increase ISO prediction skills. Both the UH-HCM and NCEP Climate Forecast System (CFS) suffer the prediction barrier over the Maritime Continent.

* School of Ocean and Earth Science and Technology Contribution Number 8154 and International Pacific Research Center Contribution Number 783.

Corresponding author address: Dr. Joshua Xiouhua Fu, International Pacific Research Center, SOEST, University of Hawaii at Manoa, 1680 East West Rd., POST Bldg. 409D, Honolulu, HI 96822.
E-mail: xfu@hawaii.edu

DOI: 10.1175/2011MWR3584.1

1. Introduction

The intraseasonal oscillation (ISO) is a dominant mode of tropical weather–climate variability with a quasi-oscillating period of 30–60 days (Madden and Julian 1972; Yasunari 1979; Wang and Rui 1990), which offers an opportunity to bridge the forecasting gap between the deterministic weather prediction (~1 week) and probabilistic climate forecast (from weeks to seasons). It has been well established that weather prediction is very sensitive to atmospheric initial conditions (Lorenz 1963, 1993, 181–184), while climate forecast is largely determined by underlying boundary conditions (Shukla 1981, 1998; Koster et al. 2000). Therefore, the weather prediction community has made great efforts to generate better atmospheric initial conditions and develop high-resolution models. On the other hand, the climate community has strived to acquire better underlying boundary conditions (e.g., sea surface temperature, soil moisture, and sea ice) and develop atmosphere–ocean–land coupled climate systems. These two communities are, respectively, sponsored by World Weather Research Program (WWRP) and World Climate Research Program (WCRP) under the auspices of World Meteorological Organization (WMO). The seamless prediction advocated by Palmer et al. (2008) and Shukla et al. (2009) calls for closer collaborations between these two communities (Moncrieff et al. 2007; Toth et al. 2007; Brunet et al. 2010; Shapiro et al. 2010; Nobre et al. 2010). The recently launched Year of Tropical Convection (YOTC) program aims to address the tropical multiscale interactions that connect weather and climate together (Waliser et al. 2009). The synergetic efforts of these two communities in coming years are expected to speed up the progresses in seamless weather–climate prediction from days to weeks, months to years, to future climate change projection beyond decades (Hurrell et al. 2009).

As a phenomenon with time scale between synoptic weather and seasonal climate, the predictability of the ISO is sensitive to both initial condition and underlying boundary condition (Krishnamurti et al. 1992; Reichler and Roads 2005; Fu et al. 2008a). In addition to the initial condition and lower boundary condition, the large-scale atmosphere–ocean interaction has been demonstrated to play a critical role in the simulation and prediction of the ISO (Fu et al. 2003; Fu and Wang 2004; Fu et al. 2007; Woolnough et al. 2007; Vitart et al. 2007). After removing high-frequency variability in the initial condition and using observed intraseasonally varying SST as lower boundary forcing, Krishnamurti et al. (1992) first demonstrated that the simulated flow fields of few selected northward-propagating ISO events over Southeast Asia still bear some similarity with the observations, even after one month of integration. Using NCEP seasonal forecast system (atmosphere-only model), Reichler and Roads (2005) carried out a suite of forecast experiments to show that, at early lead time, ISO predictability is primarily determined by initial condition, whose impact drops steadily as lead time increases. While the contribution of boundary condition on ISO predictability is secondary at the early lead time, the effect lasts much longer than that of the initial condition. Based on this finding, Reichler and Roads proposed that a fully atmosphere–ocean coupled model is the best approach to carry out operational ISO prediction. Fu et al. (2007) directly compared ISO predictability in a fully coupled model and its atmospheric component and found that interactive atmosphere–ocean coupling extends ISO predictability in the atmosphere-only model by at least a week. In a follow-up study, Fu et al. (2008a) further demonstrated that, under atmosphere-only context, the effect of the intraseasonally varying SST on ISO predictability is largely determined by the quality of initial condition. Only when the atmospheric initial condition is sufficiently accurate does the specified intraseasonally varying SST acts to extend ISO predictability. Woolnough et al. (2007) showed that coupling an atmospheric model to a 1D high-resolution oceanic mixed layer model (by including the effect of SST diurnal cycle) has longer ISO predictability than that coupled to an ocean general circulation model. This result has been confirmed by Vitart et al. (2007), Klingaman et al. (2008), and Vitart and Molteni (2009).

Early assessments of ISO practical predictability indicated that useful skills of global operational weather forecast models are 5–7 days when measured with upper-level dynamical fields (e.g., 200-hPa zonal winds), which is much shorter than its potential predictability (~1 month; Waliser et al. 2003a; Reichler and Roads 2005; Fu et al. 2007) and the skills of the statistical models (Waliser et al. 2006). This unimpressive skill of dynamical forecast is largely attributed to the failure of global models in the realistic representation of the ISO (Chen and Alpert 1990; Lau and Chang 1992; Hendon et al. 2000; Jones et al. 2000; Seo et al. 2005). With improved model physics (e.g., Sperber and Annamalai 2008; Bechtold et al. 2008) and including active air–sea coupling (Fu et al. 2007; Woolnough et al. 2007; Kim et al. 2008; W. Q. Wang et al. 2009), some global models showed useful forecasting skills of two weeks or longer (Seo et al. 2009; Vitart et al. 2007, 2008; Kim et al. 2009; Fu et al. 2008b; Lin et al. 2008; Kang and Kim 2010) when measured with a multivariate Madden–Julian oscillation (MJO) index (also called the Wheeler–Hendon index; Wheeler and Hendon 2004). This predictability is comparable to or even better than the skills of current statistical models (Waliser et al. 1999; Newman et al. 2003; Jones et al. 2004; Jiang et al. 2008).

Prediction skill can also be affected by the accuracy of initial conditions. Aforementioned dynamical ISO forecasting exercises (e.g., Hendon et al. 2000; Jones et al. 2000; Seo et al. 2005; Woolnough et al. 2007; Vitart et al. 2007; Fu et al. 2008b; Kang and Kim 2010) have used either the National Centers for Environmental Prediction Reanalysis-1 and -2 (NCEP-R1/R2) or the 15/40-yr European Centre for Medium-Range Weather Forecasts (ECMWF) Re-Analysis (ERA-15/40) datasets (Kalnay et al. 1996; Kanamitsu et al. 2002; Uppala et al. 2005) as atmospheric initial conditions. How accurate are these reanalyses in describing the ISO in the real world? Because of the sparseness of the upper-air sounding sites in the active ISO region over the Indo-Pacific warm pool and the deficiencies of the operational models in ISO simulations (e.g., Slingo et al. 1996; Waliser et al. 2003b; Lin et al. 2006), these reanalysis datasets unavoidably have various biases in representing ISO (e.g., Shinoda et al. 1999; Fu and Wang 2004; Fu et al. 2006; Tian et al. 2006). Shinoda et al. (1999) found that the ISO-related convective activities (rainfall and OLR) in the NCEP-R1 (Kalnay et al. 1996) are 2–3 factors smaller than that in the corresponding observations. Using updated forecast model and data assimilation system and fixing known problems of the NCEP-R1, Kanamitsu et al. (2002) developed an updated NCEP-R2 reanalysis. The ISO-related humidity perturbations, however, in the NCEP-R2 (Tian et al. 2006) and in the ECMWF analysis (Fu and Wang 2004; Fu et al. 2006) were still underestimated. The increased volumes of satellite observations and improved models/data assimilation techniques steadily improve the quality of reanalysis datasets in representing weather and climate variability including the ISO (e.g., Kistler et al. 2001; Andersson et al. 2005; Rienecker et al. 2009; Saha et al. 2010). On the other hand, the lack of global wind profiles' observations (particularly over the vast oceans) and an efficient constraint between the mass and flow fields in the tropics (Zagar et al. 2005), as well as the difficulties for current data assimilation systems in handling clouds/precipitation-affected radiance (Susskind 2007; Weng et al. 2007), make reanalysis datasets vulnerable to errors, particularly in the representation of tropical weather and climate variability (e.g., Mitovski et al. 2010).

How will the biases in these reanalyses affect the ISO prediction skills when they are directly used as atmospheric initial condition? Vitart et al. (2007) found that ISO prediction skill is higher when initialized with the ERA-40 than that initialized with the ERA-15, because the ERA-40 has stronger ISO than that of the ERA-15. Vintzileos and Pan (2007) also showed that ISO prediction skills initialized with the NCEP Global Data Assimilation System (GDAS) is consistently higher than that initialized with the NCEP-R2 (Kanamitsu et al. 2002) because of the better representation of the ISO in the GDAS than that in the NCEP-R2. Using the NCEP-R1[1] as initial condition, Fu et al. (2009) found that the ISO prediction skill in 2004 summer season is only about a week over the global tropics (30°S–30°N) and Southeast Asia (10°–30°N, 60°–120°E) for the associated rainfall and 850-hPa zonal winds. A prototype signal-recovery approach was utilized to enhance the ISO in the initial condition. When the ISO amplitudes were tripled in the original reanalysis, the resultant prediction skills of the ISO increased to 25 days for 850-hPa zonal winds and 15 days for rainfall over both Southeast Asia and the global tropics.

The present study is an extension of Fu et al. (2009). The objectives of this study are threefold: 1) document the biases of three reanalysis datasets in describing the ISO, 2) explore the ways to improve the representation of the ISO in initial condition, and 3) assess the impacts of different initial conditions on ISO prediction skills. The present forecast experiments cover 5 summer seasons from 2004 to 2008. In addition to the NCEP-R1 used in Fu et al. (2009), NCEP-R2 and ECMWF Re-Analysis Interim (ERA-Interim; Uppala et al. 2008) were also used to initialize the forecasts. An enhanced-divergence-nudging method is found to generate better initial conditions. To assess the impacts of small-scale synoptic disturbances on ISO prediction, one set of experiments that excludes synoptic disturbances in original NCEP-R2 are also conducted. To check the possible model dependence of our findings, the forecasts from the NCEP Climate Forecast System (CFS; Saha et al. 2006) in 2008 summer have been compared with the forecasts from the ECHAM4–University of Hawaii hybrid coupled model (UH-HCM).

This paper is structured as follows. The UH-HCM and forecast experiment design are given in section 2. Section 3 documents the biases of three reanalysis datasets in the description of the ISO. Section 4 assesses the impacts of an enhanced-divergence-nudging method on initial condition and ISO prediction. Section 5 examines to what degree the signal-recovery method and synoptic disturbances in initial conditions affect ISO prediction. The last section summarizes our major findings and discusses possible future studies.

2. Model description and forecast experiment design

The model used to carry out the forecast experiments is a hybrid atmosphere-ocean coupled model (UH-HCM),

[1] As revealed in Shinoda et al. (1999), the convective activity (rainfall) associated with both northward- and eastward-propagating ISO in the 2004 summer is still 2–3 factors smaller than the observed [Fig. 1 in Fu et al. (2009)].

developed at the International Pacific Research Center at the University of Hawaii (Fu and Wang 2004). The atmospheric component is a general circulation model (ECHAM4), developed at Max Planck Institute for Meteorology in Germany (Roeckner et al. 1996). The mass flux scheme of Tiedtke (1989) is used to represent the deep, shallow, and midlevel convection with Nordeng's (1995) modified closure. The ocean component is an intermediate tropical upper-ocean model developed at the University of Hawaii (Wang et al. 1995; Fu and Wang 2001), which comprises a mixed layer, in which the temperature and velocity are vertically uniform, and a thermocline layer in which temperature decreases linearly from the mixed layer base to the thermocline base. Both layers have variable depth and exchange mass and heat through entrainment and detrainment.

The global atmospheric model has been coupled to the ocean model over the tropical Indian and Pacific Oceans without using heat flux correction. Outside the tropical Indian and Pacific Oceans, sea surface temperature is specified as climatologically monthly-mean SST averaged from the 16-yr Atmospheric Model Intercomparison Project (AMIP) SST (1979–94). In all forecast experiments, a restart file from a long-term coupled run has been used to initialize the nudging integration, which in turn generates initial conditions for all forecast experiments.

During the nudging integration, three reanalysis datasets (e.g., NCEP-R1, -R2, and ERA-Interim) are nudged into the UH-HCM. Different nudging coefficients are used for different variables (vorticity, divergence, temperature, and surface pressure). The default coefficients in the standard ECHAM4 AGCM are those used by Danish Meteorological Institute (DMI),[2] in which vorticity is strongly nudged, but divergence is very weakly nudged. This may be good for the midlatitude but is problematic in the tropics (Jeuken et al. 1996). To alleviate this weakness of the DMI nudging, divergence nudging strength has been increased in this study, which is referred as enhanced divergence nudging (EDN).

A signal-recovery method has been proposed to augment the underestimated ISO signal in the original reanalysis (Fu et al. 2009). The procedure is as following: first, 30–90-day variability is extracted from 1-yr original reanalysis with harmonic analysis; second, the extracted ISO signal is augmented by doubling its magnitude; then, the 30–90-day variability in the original reanalysis is replaced with augmented ISO signal. Finally, the modified reanalysis is nudged into the UH-HCM with the EDN nudging to generate a new product: *signal-recovered reanalysis*.

[2] These nudging coefficients were used in Fu et al. (2009).

In this study, most forecast experiments have targeted five summer seasons (2004–08). Each year, 16 forecasts have been initiated every 10 days from 1 May to 31 September. Ten ensembles have been executed for each forecast. The way to generate ensemble initial condition is the same as that used in our previous predictability study (Fu et al. 2007). Each forecast is integrated for 60 days. To measure the prediction skills, 120-day observations [e.g., Tropical Rainfall Measuring Mission (TRMM) rainfall and 850-hPa zonal winds from the NCEP-R2] before the initial dates have been concatenated to the 60-day ensemble-mean forecasts. Then, harmonic analysis is used to extract intraseasonal signals (30–90 day) from the merged 180-day time series and the corresponding observations. Finally, the anomaly correlation coefficients (ACC; Wilks 2005) between the forecasts and the observations are calculated during the 60-day forecast period, respectively, for the global tropics (30°S–30°N) and Southeast Asia (10°–30°N, 60°–120°E). As in Fu et al. (2009), a moderate value of the ACC (0.4) was used to measure ISO prediction skill in days (e.g., Jones et al. 2000; Fu et al. 2007). As an alternative to the aforementioned measure, the prediction skills of the Wheeler–Hendon index (Lin et al. 2008) were also presented.

3. Biases of global reanalysis datasets in describing the ISO

Three reanalysis datasets: the NCEP-R1, -R2, and ERA-Interim were used to initialize our forecast experiments. Although similar observational data may have been used as input to generate these reanalysis datasets, the different model physics and data assimilation techniques will result in different reanalysis products. For example, when observed rainfall was assimilated into the ERA-Interim (Andersson et al. 2005; Simmons et al. 2007), the reanalysis rainfall produced in the forecast cycle has much higher spatial pattern correlation with the observations than that without assimilating observed rainfall (Table 1). In this study, the biases of three reanalysis datasets in describing the ISO were briefly documented and possible ways to alleviate the biases were explored.

Over the vast tropical oceans, available in situ observations are very limited. It is difficult to construct spatially continuous "ground truth" based purely on in situ observations, particularly for the ISO, whose active region is over the tropical Indo-western Pacific Oceans. Therefore, we utilize one of the well-validated satellite retrievals, TRMM rainfall, as ground truth to assess the quality of three reanalysis datasets.

Figure 1 shows the spatial patterns of intraseasonal (30–90 day) rainfall standard deviation from TRMM, the NCEP-R1, -R2, and ERA-Interim averaged for the

TABLE 1. Averaged daily spatial pattern correlations of intraseasonal (30–90 day) rainfall anomalies during boreal summer [May–October (MJJASO)] between three reanalysis datasets and TRMM observations over tropical Indo–western Pacific Oceans (30°S–30°N, 40°E–140°W).

	NCEP-R1	NCEP-R2	ERA-Interim
2004	0.60	0.46	0.80
2005	0.57	0.42	0.78
2006	0.59	0.47	0.80
2007	0.56	0.50	0.78
2008	0.55	0.48	0.77
Mean	0.58	0.47	0.79

2004–08 summer seasons. Both the NCEP-R1 (Figs. 1b,e) and ERA-Interim (Figs. 1d,g) underestimate the intensity of the observed intraseasonal variability over almost the entire Indo-western Pacific Oceans. On the other hand, the total intraseasonal variability in the NCEP-R2 (Figs. 1c,f) is higher than the observed, particularly over the Bay of Bengal and the eastern Arabian Sea. Table 1 gives the summer-mean ACCs of intraseasonal rainfall anomalies between three reanalysis datasets and the observations from 2004 to 2008. The 5-yr means are 0.58, 0.47, and 0.79 for the NCEP-R1, -R2, and ERA-Interim, respectively. As expected, the ERA-Interim has the best rainfall spatial pattern. It is interesting to note that intraseasonal rainfall pattern in the NCEP-R1 is actually better than that in the NCEP-R2 even though the latter has much stronger variability than the former.

As for ISO prediction, the quality of near-equatorial ISO in the reanalyses is essential because the ISO has a significant eastward-propagating component along the equator year-round. Even in boreal summer, the dominant northward propagation of the ISO starts from the equator. Because of the lack of an efficient constraint between the mass and flow fields (like the quasigeostrophic balance in the midlatitude) and very limited upper-air soundings, the equatorial region has been a very difficult area for data assimilation (e.g., Zagar et al. 2005). It is imperative to take a close look of the ISO near the equator in various reanalysis products. A brief description and statistics of seven products used in the present study are given in Table 2. For illustration purpose, Fig. 2 shows the Hovmöller diagrams of total rainfall and the associated intraseasonal variability along the equator in 2004 summer from TRMM observations, the NCEP-R2 and ERA-Interim along with the nudged R2, nudged ERA-Interim, and signal-recovered R2/ERA-Interim (Table 2). In the observations (Fig. 2a), 4–5 ISO events develop in the Indian Ocean and propagate eastward into the western Pacific. The NCEP-R2 (Fig. 2b) captures some of the observed features but is not as well organized as the observed events. Too many and too strong high-frequency westward-propagating disturbances exist in the R2, particularly in the western Pacific. An obvious fictitious westward-propagating ISO event exists in July over the Indian Ocean. The correlation coefficient, which measures the similarity of the longitude–temporal evolutions between the reanalysis ISO rainfall anomaly and the observations, is about 0.5. The ERA-Interim (Fig. 2c) has very similar spatial–temporal evolutions as the observations but with the amplitude underestimated. The correlation coefficient with the observations reaches 0.88.

After nudging the NCEP-R2 into the UH-HCM (Fig. 2d), the too strong small-scale convection presented in the original R2 has been mitigated. The fictitious westward-propagating ISO event in July over the Indian Ocean disappeared. The correlation coefficient with the observations increases to 0.58. This improvement after nudging is likely due to the better representation of convective processes in the UH-HCM than that in the NCEP model because the associated dynamical fields in both cases are very similar. After doubling the intraseasonal signals in both the NCEP-R2 and ERA-Interim and nudging into the UH-HCM, the resultant products own stronger intraseasonal variability than the nudged reanalyses (Figs. 2e,f), which are called signal-recovered NCEP-R2 and ERA-Interim. The signal-recovered ERA-Interim, however, has lower correlation with the observations than the original reanalysis. The underlying reasons deserve further study.

Table 2 also shows that the ERA-Interim has the best spatial–temporal evolutions among the 3 reanalyses with 5-yr mean correlation coefficient reaching 0.85. The NCEP-R1 (0.58) is slightly, but consistently, better than the NCEP-R2 (0.51) in this regard. It looks that the quality of the NCEP-R1 in representing ISO is in between the NCEP-R2 and ERA-Interim. Therefore, most following analyses and experiments will be done by using the NCEP-R2 and ERA-Interim. We expected that the results with the NCEP-R1 will also fall in between the NCEP-R2 and ERA-Interim. After nudging the NCEP-R2 and ERA-Interim into the UH-HCM, the correlation coefficient increases for the R2 (from 0.51 to 0.56), but deceases for the ERA-Interim (from 0.85 to 0.79). After doubling ISO variability in the NCEP-R2/ERA-Interim and nudging to the UH-HCM, the correlation coefficient increases from 0.56 to 0.62 for the R2 but decreases from 0.79 to 0.76 for the ERA-Interim. The reasons resulting in the decrease of correlation for the ERA-Interim will be a future research topic.

The above assessment reveals that the spatial–temporal evolutions of the ISO in the ERA-Interim are better than that in the NCEP-R2, but with the amplitude underestimated (Figs. 1d,g, and Fig. 2c). For the R2, the quality of the ISO after strength doubling is systematically improved over that without doubling. For the ERA-Interim,

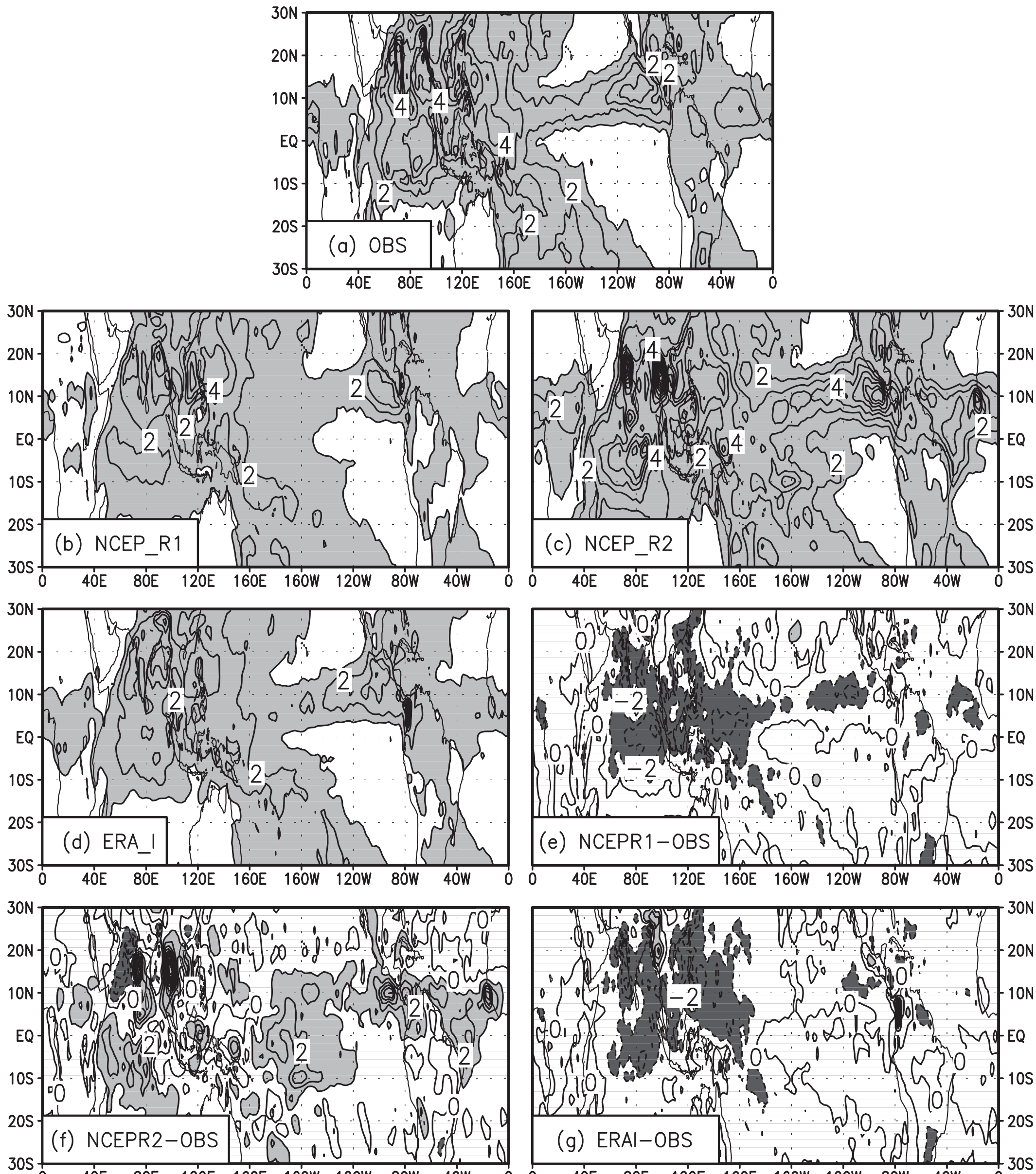

FIG. 1. Spatial patterns of intraseasonal (30–90 day) rainfall standard deviation (mm day^{-1}) for (a) TRMM observations (OBS), (b) NCEP-R1, (c) NCEP-R2, and (d) ERA-Interim averaged over the 2004–08 summer seasons (MJJASO) along with the differences of (e) NCEP-R1 − OBS, (f) NCEP-R2 − OBS, and (g) ERA-I − OBS.

however, the results are kind of mixing. How will these differences in various reanalyses and their modifications impact the prediction skills of the ISO when they are used to initialize ISO prediction? The following two sections aim to answer this question.

4. EDN and its impact on ISO prediction

In section 2, we have introduced two nudging methods: the DMI and the EDN. This section will assess in what degree different nudging methods impact the initial conditions and ISO prediction skills.

Figure 3 shows the time series of daily spatial pattern correlations between nudged rainfall and the observations in the 2004 summer. For both the NCEP-R2 and ERA-Interim, the EDN nudging results in significantly higher pattern correlations of daily total (Figs. 3a,b) and intraseasonal anomaly (Figs. 3c,d) than that with the DMI nudging. The improvements on intraseasonal components are much more obvious (Figs. 3c,d). Figure 4 gives

TABLE 2. Correlation coefficients of intraseasonal (30–90 day) rainfall anomalies during boreal summer [May–October (MJJASO)] along the equator (averaged between 10°S and 10°N) between different reanalysis datasets and observations. NCEP-R1, NCEP-R2, and ERA-Interim denote three original reanalyses; Nudg-ERAI and Nudg-R2 are products after nudging ERA-Interim and NCEP-R2 into UH-HCM with the EDN nudging; Nudg-2xERAI and Nudg-2xR2 are products after nudging ERA-Interim and NCEP-R2 with ISO signal doubled using the EDN nudging, which are also called signal-recovered ERA-Interim and NCEP-R2. The horizontal resolutions of UH-HCM, NCEP-R1, NCEP-R2, and ERA-Interim are T30, T62, and T255. In above analysis, all data have been regridded onto 2.5° × 2.5° resolution.

	NCEP-R1	NCEP-R2	ERA-I	Nudg-ERAI	Nudg-R2	Nudg-2xERAI	Nudg-2xR2
2004	0.60	0.50	0.88	0.79	0.58	0.77	0.66
2005	0.64	0.49	0.86	0.80	0.60	0.75	0.65
2006	0.61	0.53	0.84	0.80	0.51	0.75	0.53
2007	0.54	0.50	0.82	0.80	0.52	0.76	0.61
2008	0.48	0.54	0.84	0.78	0.60	0.75	0.65
Mean	0.58	0.51	0.85	0.79	0.56	0.76	0.62

an example on 10 August 2004 for daily total rainfall from the observations and a variety of nudging experiments when the NCEP-R2 and ERA-Interim are, respectively, used. Compared to the observations (Fig. 4a), the DMI nudging produces too much rainfall in the equatorial Indian Ocean and western Pacific ITCZ (~10°N) near the date line for both reanalyses (Figs. 4b,c), at the same time, it significantly underestimates

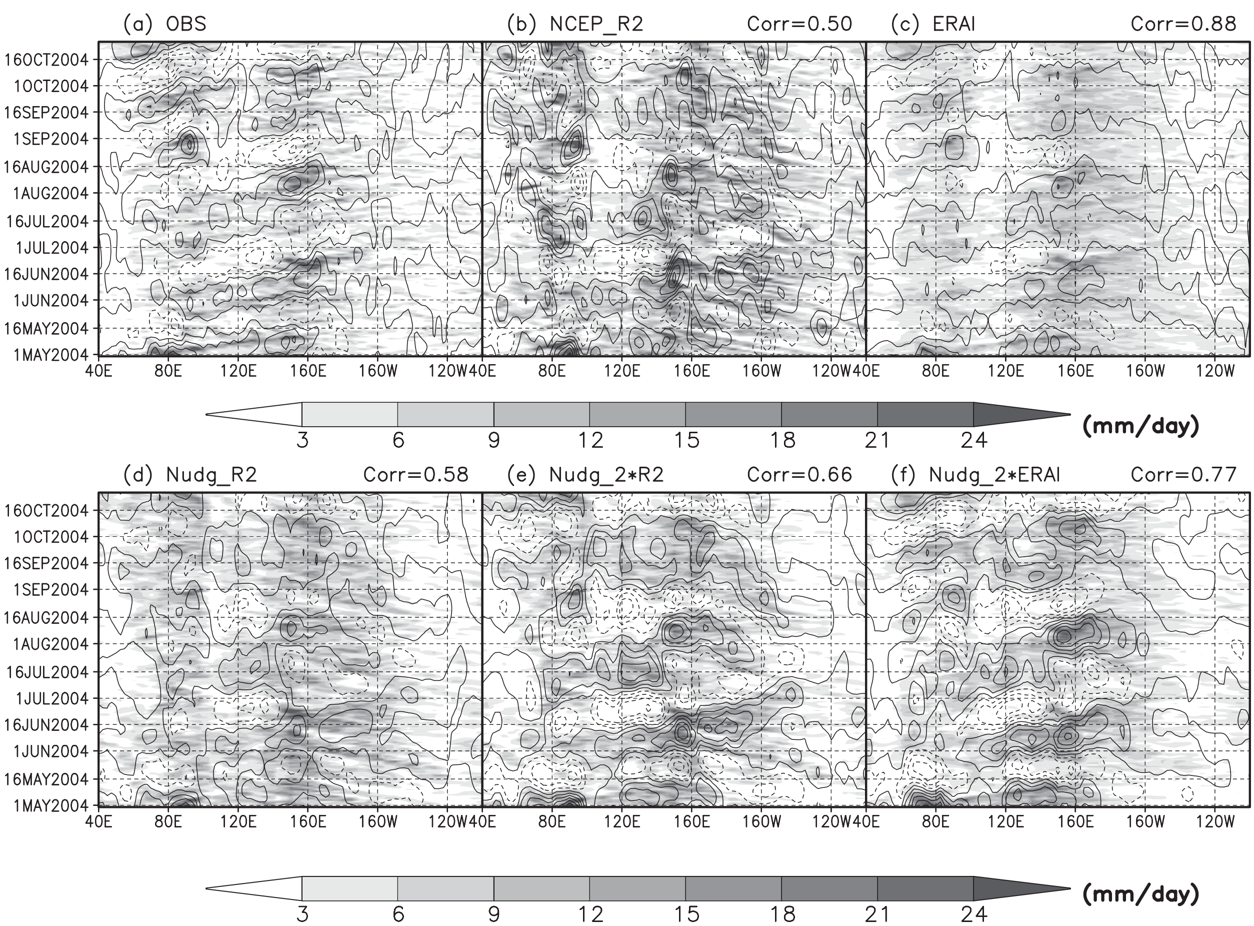

FIG. 2. Longitude–time evolutions of daily total rainfall (shaded) and associated intraseasonal (30–90 day) variability [contours, contour interval (CI): 1 mm day^{-1}] averaged between 10°S and 10°N in the 2004 summer from (a) TRMM observations (OBS), (b) NCEP-R2, (c) ERA-Interim, (d) Nudged NCEP-R2, (e) signal-recovered NCEP-R2, and (f) signal-recovered ERA-Interim.

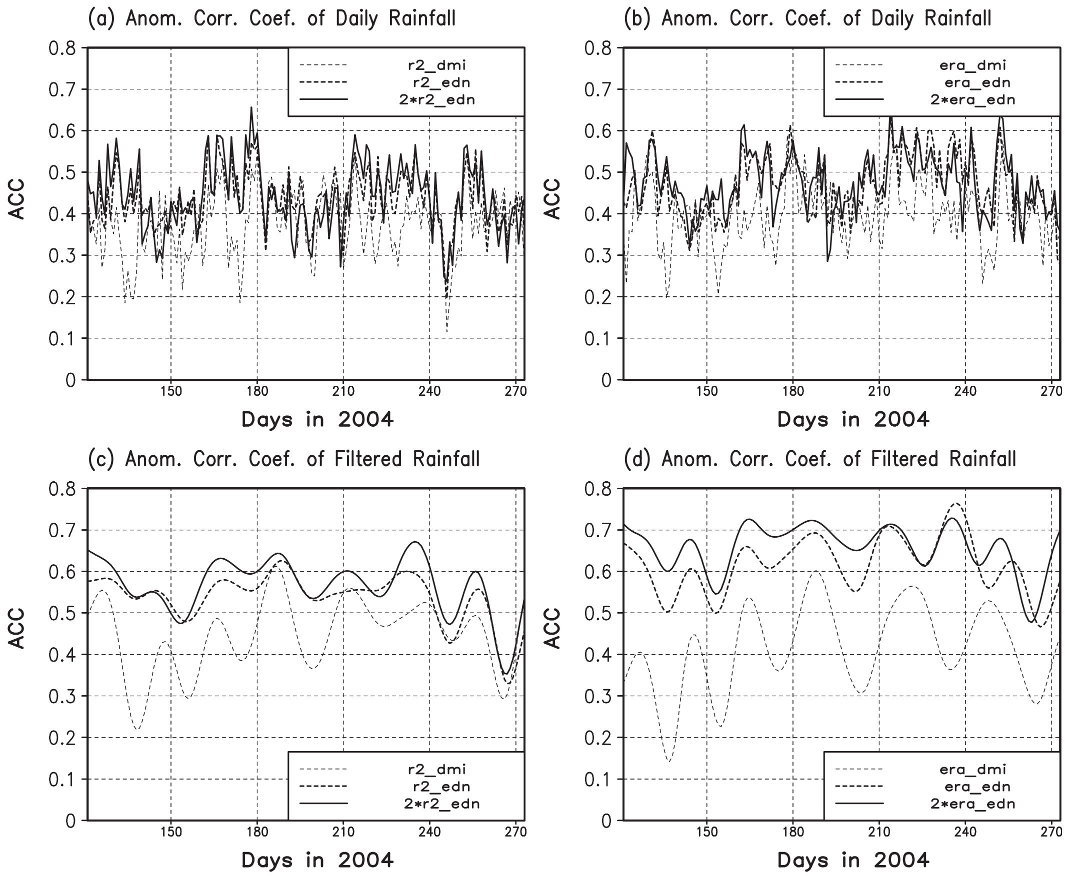

FIG. 3. Pattern correlations over (30°S–30°N, 40°E–140°W) between the nudged rainfall and the observations in the 2004 summer: (a) daily total rainfall with the NCEP-R2 [r2_dmi used loose divergence nudging; r2_edn used the EDN; 2*r2_edn doubled ISO signals in the original NCEP-R2 and used the EDN]. (b) Daily total rainfall with the ERA-Interim [era_dmi, era_edn, and 2*era_edn have similar meanings as in (a), but with the ERA-Interim]. (c) As in (a), but for intraseasonally filtered rainfall. (d) As in (b), but for intraseasonally filtered rainfall.

the northwest–southeast-tilted rainbelt in the western edge of tropical Pacific. On the other hand, the EDN nudging (Figs. 4d,e) considerably alleviates the aforementioned biases: reducing rainfall in the equatorial Indian Ocean and shifting the western-Pacific ITCZ rainfall westward. The resultant rainfall pattern is very similar with the observed one (Fig. 4a). After doubling ISO signals (Figs. 4f,g), the equatorial Indian Ocean rainfall is further reduced. The overall pattern correlations are very similar as that with the EDN nudging (Fig. 3). This result demonstrated that the EDN nudging produces much better tropical rainfall in the initial conditions than that with the default DMI nudging in the ECHAM model.

By using two different nudging methods, a total of six sets of initial conditions are generated for the three reanalyses: the NCEP-R1, -R2, and ERA-Interim in the 2004 summer. Six sets of forecasts have been produced with respective initial conditions. Each set has 16 forecasts starting every 10 days to cover an entire summer (from 1 May to 31 September); each forecast has 10 ensembles. We calculated the prediction skill of each forecast with 10-ensemble mean, then taking the average skill of 16 forecasts to represent the skill under a specific initial condition. The variables used to calculate the skills are intraseasonally filtered 850-hPa zonal winds (U850) and rainfall. As in Fu et al. (2009), forecast skills have been assessed over the global tropics and Southeast Asia.

Figure 5 summarizes the intraseasonal prediction skills of U850 and rainfall over two different domains under six different initial conditions. Two features stand out: the overall skills initialized with three reanalysis datasets are similar and the skills are largely separated by the usage of different nudging methods. As we found in Fu et al. (2009), the prediction skills initialized with the NCEP-R1, -R2, and ERA-Interim are about a week when the DMI nudging is used. Usually, the forecast skills of U850 are slightly longer than that of rainfall. The EDN nudging extends the rainfall prediction skills

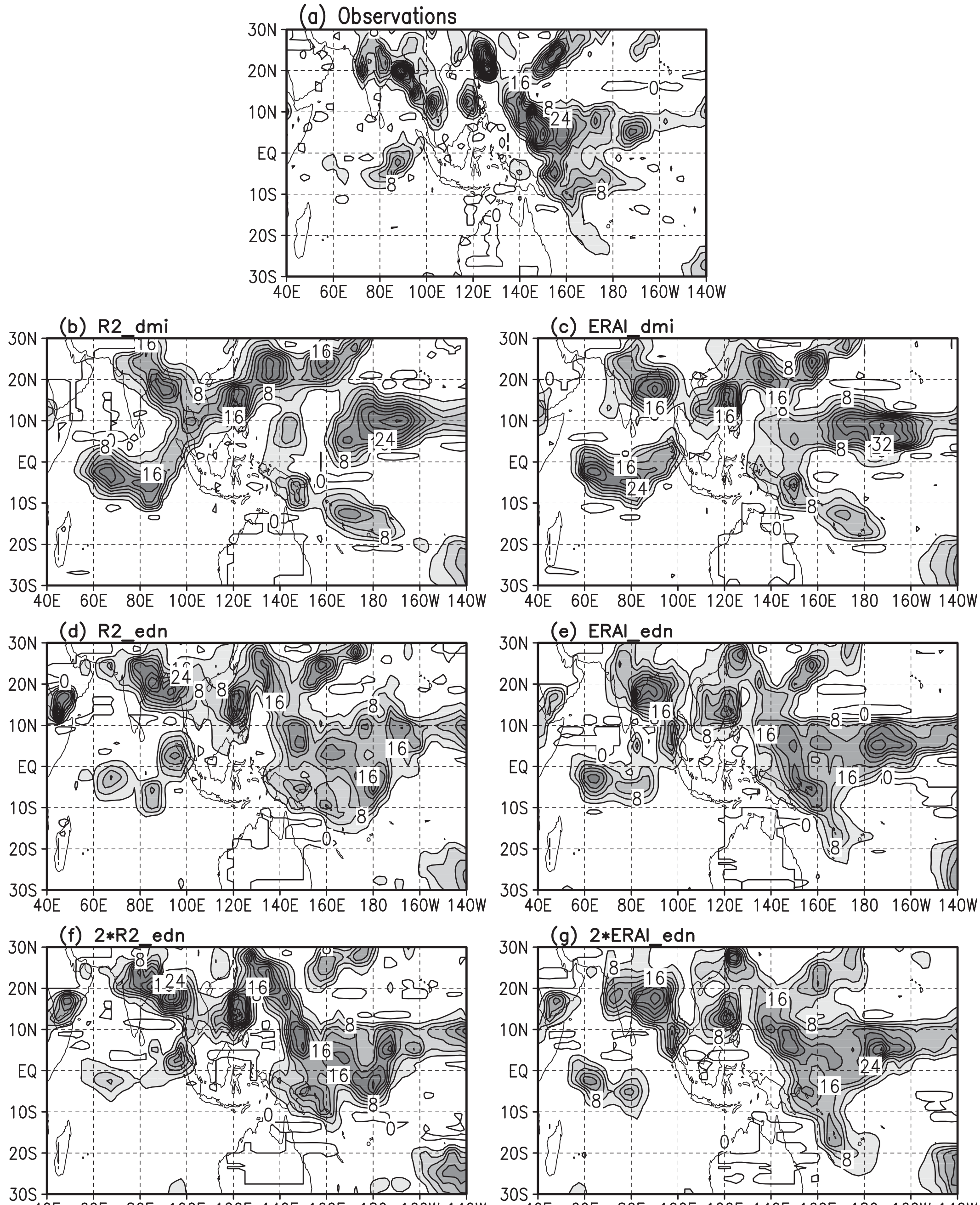

FIG. 4. Spatial patterns of daily rainfall (CI: 2 mm day^{-1}) on 11 Aug 2004 from (a) the observations, (b) nudged NCEP-R2 with loose divergence nudging (dmi), (c) nudged ERA_Interim with loose divergence nudging, (d) nudged NCEP-R2 with EDN, (e) nudged ERA-Interim with enhanced EDN, (f) nudged NCEP-R2 with ISO signal doubled and EDN, and (g) nudged ERA-Interim with ISO signal doubled and EDN.

by 2–4 days (Figs. 5b,d) and considerably improves the skills of U850 (Figs. 5a,c); about a 5–10-day extension over the global tropics and over Southeast Asia. Among the three reanalyses, the ERA-Interim has obviously better skills than the NCEP-R1/R2 except for rainfall over Southeast Asia. This finding demonstrates that the EDN nudging leads to better initial conditions, thus improving the overall ISO prediction skill. All results presented in remaining part of this study were obtained with the EDN nudging.

The skills of ISO prediction, however, are not uniformly distributed within a season, but change significantly as

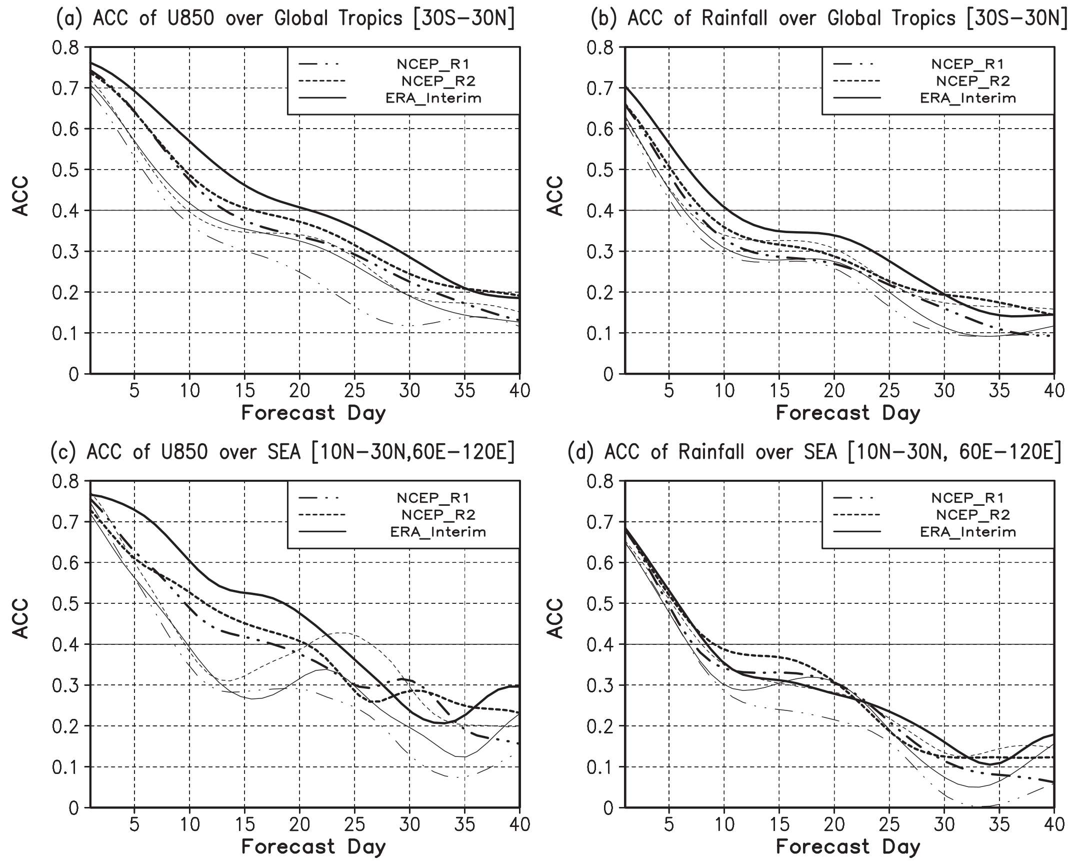

FIG. 5. ISO prediction skills initialized with three nudged reanalysis datasets: The NCEP-R1, NCEP-R2, and ERA-Interim with two different nudging methods (loose divergence nudging: dashed lines, EDN: solid line): (a) ACC of U850 over the global tropics, (b) ACC of rainfall over the global tropics, (c) ACC of U850 over Southeast Asia, and (d) ACC of rainfall over Southeast Asia.

a function of initial dates. Figure 6 shows the temporal variations of ISO prediction skills over the global tropics in 2004 summer. The skills are highest when forecasts started in late June/early July no matter using the NCEP-R2 or ERA-Interim as initial conditions or measuring the skills with U850 or rainfall. On the other hand, the prediction skills are lowest when forecasts started around 21 July. What cause these large temporal variations of prediction skills? Checking back to Fig. 2, we found that, when initial ISO-related convection locates over the Maritime Continent, the resultant prediction skills are lowest. After initial ISO-related convection moves to the east of the Maritime Continent, the prediction skills are highest.

In what degree are the above findings model dependent? Fully addressing this issue requires well-coordinated multimodel intercomparisons (e.g., B. Wang et al. 2009). To offer a preliminary answer to this question, we compared the 2008 summer forecasts between the UH-HCM and the NCEP-CFS. Figure 7 shows the prediction skills of rainfall and U850 over the global tropics from these two models. Both forecasts were initialized with the NCEP-R2. Although the UH-HCM and the CFS have very different physical schemes, the temporal variations of the skills are very similar. After checking the Hovmöller diagram of the observed total rainfall and the associated intraseasonal variability along the equator in 2008 summer (figure not shown), it is also found that the lowest skills correspond to initial ISO-related convection over the Maritime Continent, but the highest are after the convection moving to the east of the Maritime Continent. Similar phase dependence is also found for the ISO prediction over Southeast Asia (Fig. 8). These results point out that the Maritime Continent is a prediction barrier for both the UH-HCM and the CFS (Vintzileos and Pan 2007). A similar barrier has been reported for the ECMWF forecast system, too (Vitart et al. 2007). This prediction barrier is likely caused by both model deficiencies and inadequate initial conditions. Further in-depth studies are needed to sort this out.

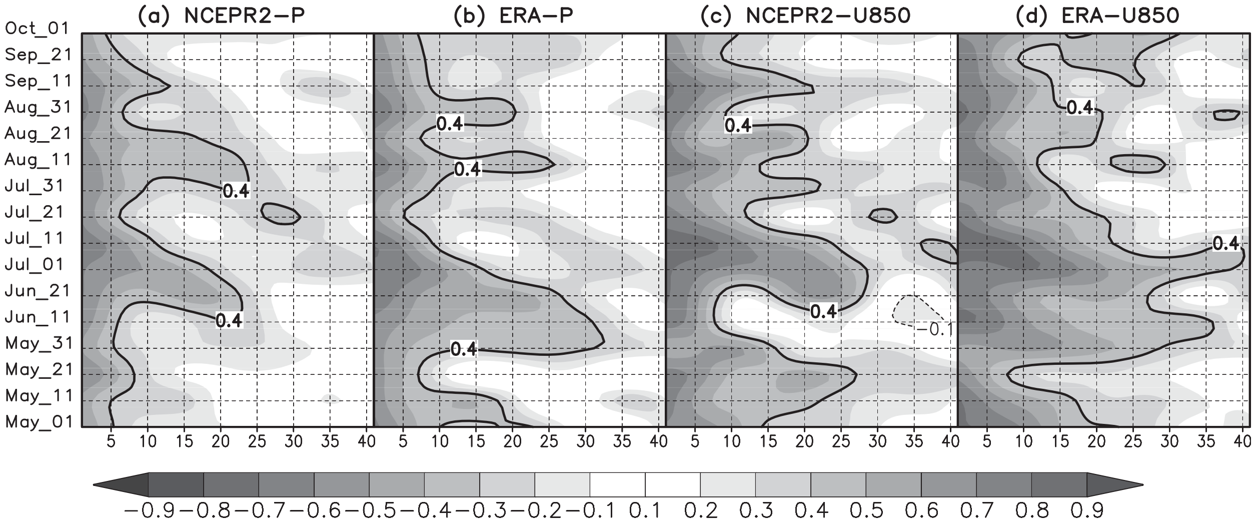

FIG. 6. ACC of forecasted ISO against the observations over global tropics in the 2004 summer as a function of initial dates: (a) skills of filtered rainfall initialized with the nudged NCEP-R2, (b) skills of filtered rainfall initialized with the nudged ERA-Interim, (c) skills of filtered U850 initialized with the nudged NCEP-R2, and (d) skills of filtered U850 initialized with the nudged ERA-Interim.

Comparison of Figs. 8a,b suggests that the overall rainfall prediction skill in the UH-HCM is higher than that in the NCEP CFS. Taking the prediction skill initiated on 31 August 2008 as an example, the skill of the CFS (Fig. 8a) changes from positive to negative after about 10 days, while the skill of the UH-HCM (Fig. 8b) stays positive for more than 40 days. To understand the cause of this skill difference, Fig. 9 gives the latitude–time evolutions of the forecasted intraseasonal rainfall anomalies averaged over 60°–120°E from the CFS and the UH-HCM along with the observations. Initially, a north–south rainfall dipole is observed in this sector with a wet phase near the equator and a dry phase over Southeast Asia. The near-equatorial wet phase gradually moves northward to Southeast Asia, followed by a northward-propagating dry phase. The northward-propagating wet phase forecasted by the CFS (Fig. 9a) is way too slow in comparison to the observations, which may be due to the underestimated air–sea coupling (W. Q. Wang et al. 2009). Too slow ISO propagations in

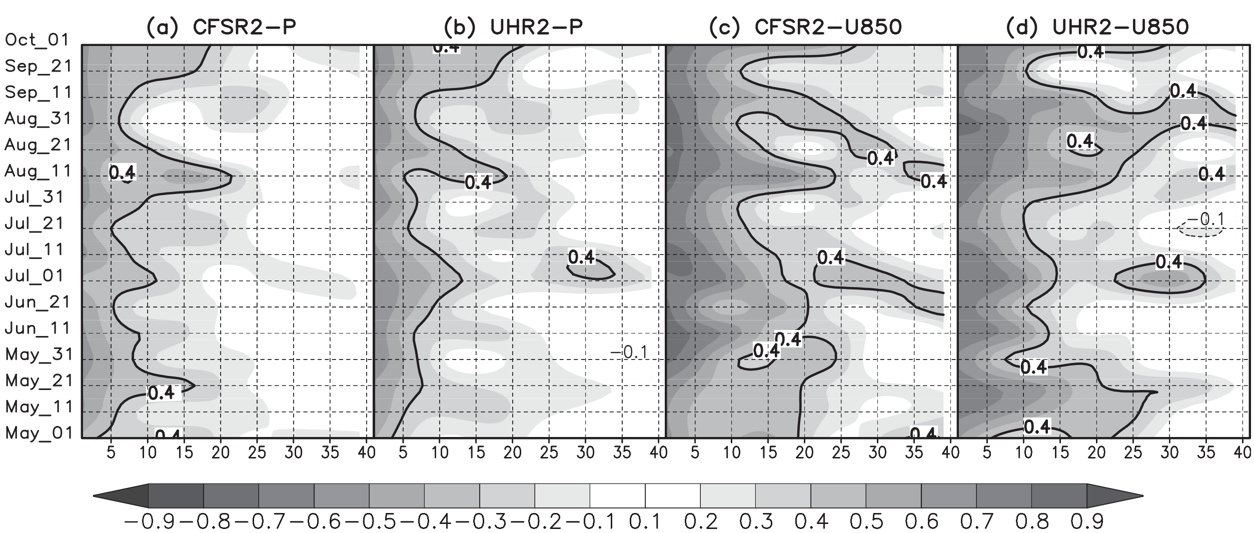

FIG. 7. ACC of forecasted ISO against the observations over global tropics in the 2008 summer as a function of initial dates: (a) skills of forecasted rainfall by the CFS, (b) skills of forecasted rainfall by the UH-HCM, (c) skills of forecasted U850 by the CFS, and (d) skills of forecasted U850 by the UH-HCM.

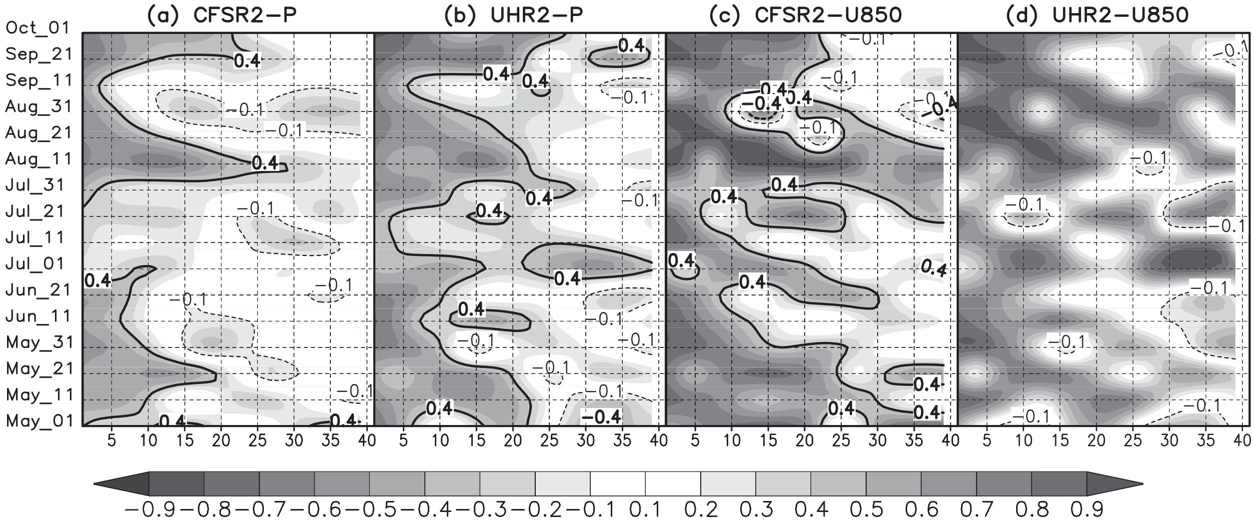

FIG. 8. As in Fig. 7, but over Southeast Asia.

the CFS have also been reported in long-term free integrations (e.g., Pegion and Kirtman 2008; Achuthavarier and Krishnamurthy 2009). On the other hand, the UH-HCM initiated with either the NCEP-R2 (Fig. 9b) or the ERA-Interim (Fig. 9c) produces a much better northward-propagating wet phase and the follow-up dry phase although the southward-propagating wet phase is overestimated.

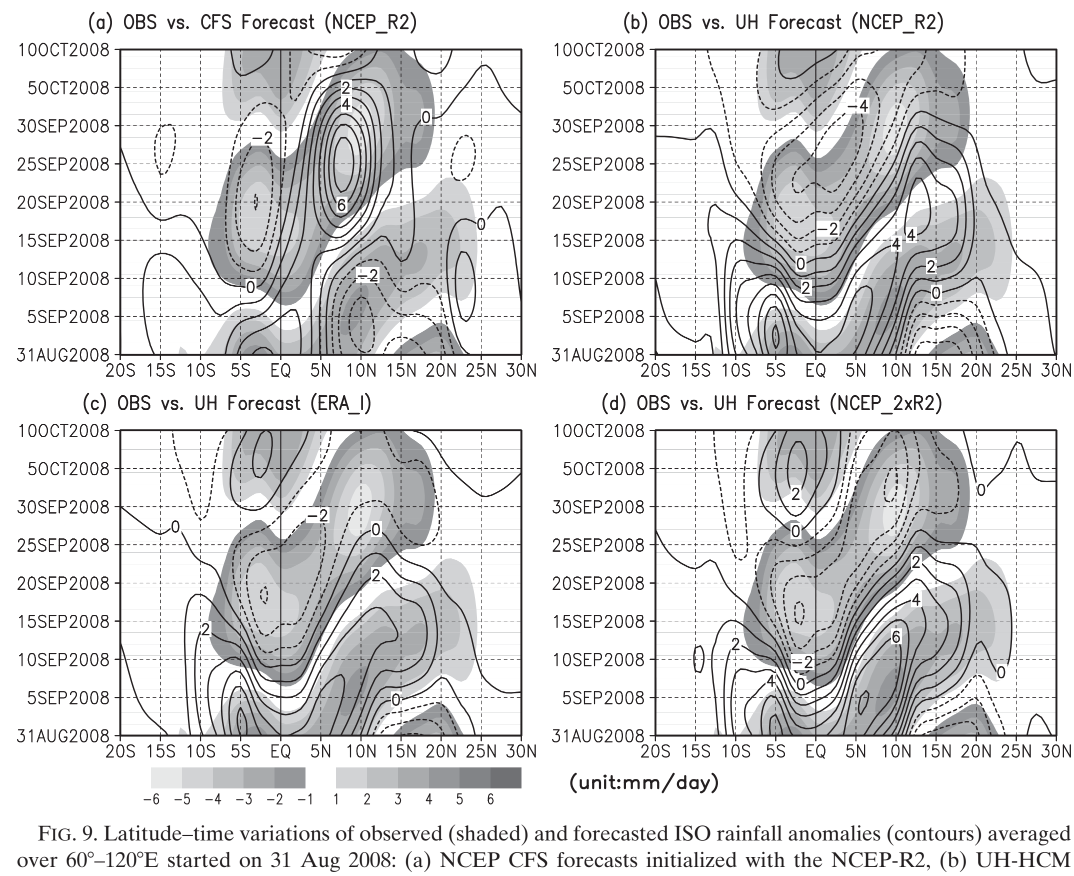

FIG. 9. Latitude–time variations of observed (shaded) and forecasted ISO rainfall anomalies (contours) averaged over 60°–120°E started on 31 Aug 2008: (a) NCEP CFS forecasts initialized with the NCEP-R2, (b) UH-HCM forecasts initialized with the nudged NCEP-R2, (c) UH-HCM forecasts initialized with nudged ERA-Interim, and (d) UH-HCM forecasts initialized with signal-recovered NCEP-R2.

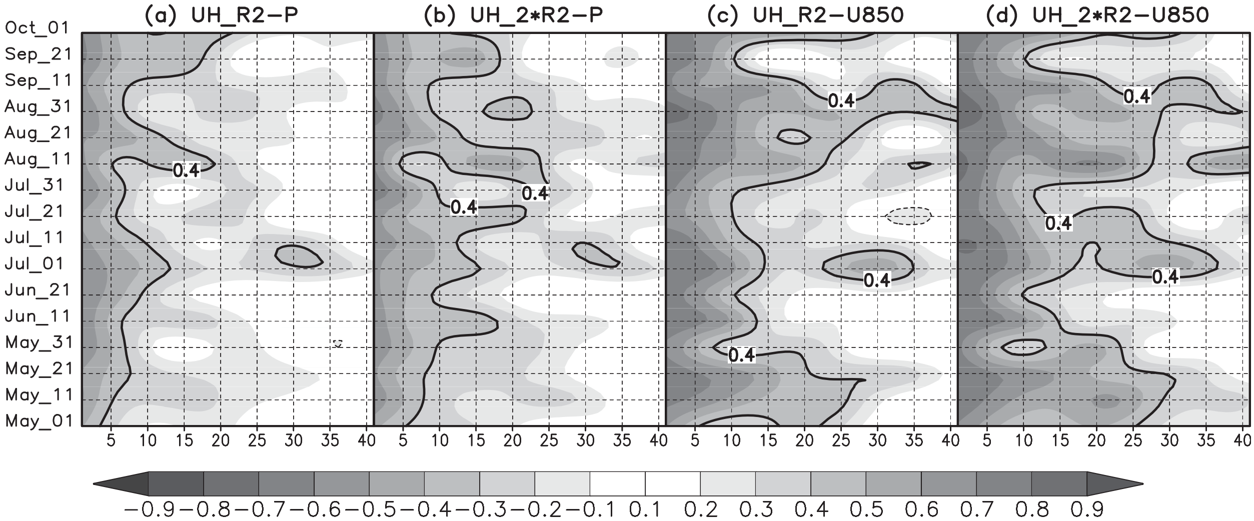

FIG. 10. ACC of forecasted ISO against the observations over the global tropics in the 2008 summer as function of initial dates: (a) skills of intraseasonal rainfall initialized with the nudged NCEP-R2, (b) skills of intraseasonal rainfall initialized with signal-recovered NCEP-R2, (c) skills of intraseasonal U850 initialized with the nudged NCEP-R2, and (d) skills of intraseasonal U850 initialized with signal-recovered NCEP-R2.

5. A signal-recovery method and its impact on ISO prediction

When intraseasonal signal of the NCEP-R1 in 2004 summer was recovered to be comparable to the observations, the resultant ISO prediction skill increased accordingly (Fu et al. 2009). A natural question arises: what will happen for other years and with other reanalysis datasets? To answer this question, extended forecast experiments have been conducted for five continuous summers (2004–08) initialized with signal-recovered NCEP-R2 and ERA-Interim reanalyses. As shown in Fig. 2 and Table 2, the quality of the ISO in the signal-recovered NCEP-R2 is much better than that in the original reanalysis; whereas the result of the signal-recovered ERA-Interim is a kind of mixing. Will these so-called signal-recovered initial conditions lead to better intraseasonal prediction skills?

The present section aims to address this question. First, let us continue the case that was initialized on 31 August 2008. Figure 9d shows the UH-HCM forecast initialized with signal-recovered NCEP-R2. The forecast looks better than that initialized with the nudged NCEP-R2 (Fig. 9b). After recovering the ISO signal in the initial conditions (Fig. 9d), the northward-propagating component is strengthened and the southward component weakened. The resultant forecast (Fig. 9d) not only well captures the northward-propagating wet phase and the follow-up dry phase, but also reproduces the reinitiation of a new wet phase near the equator even after one month.

Figure 10 shows the temporal variations of ISO prediction skills in the 2008 summer over the global tropics initialized, respectively, with the nudged and signal-recovered NCEP-R2. For both rainfall and U850, the forecasts initialized with the signal-recovered reanalysis (Figs. 10b,d) have obviously better skills than that initialized with the nudged reanalysis (Figs. 10a,c). The rainfall prediction skills have been significantly extended particularly for two cases: one initialized on 21 July and the other initialized on 11 June (Figs. 10a,b). Since these dates correspond to the periods when the ISO moves over the Maritime Continent, the differences between the forecasts initialized with the nudged NCEP-R2 and that with signal-recovered NCEP-R2 suggest that ISO-related convection over the Maritime Continent has been misrepresented in the NCEP-R2 and improved representation of the ISO over the Maritime Continent extends ISO prediction skills.

Figure 11 compares the prediction skills of rainfall and U850 over Southeast Asia in the 2008 summer initialized with the nudged and signal-recovered NCEP-R2. The forecasts initialized with signal-recovered reanalysis have systematically higher skills than that initialized with the nudged reanalysis for both rainfall and U850. Largest extensions of ISO-related rainfall prediction skills occur for the cases initialized on 11 and 21 July 2008 (Figs. 11a,b). The useful prediction skills initialized with the nudged NCEP-R2 for these two cases are mostly within 5 days (Fig. 11a), being extended to more than 25 days when the signal-recovered reanalysis is used as initial condition. The improved skills primarily result from faster and more coherent northward propagation of the ISO in the later cases, as illustrated in Fig. 9.

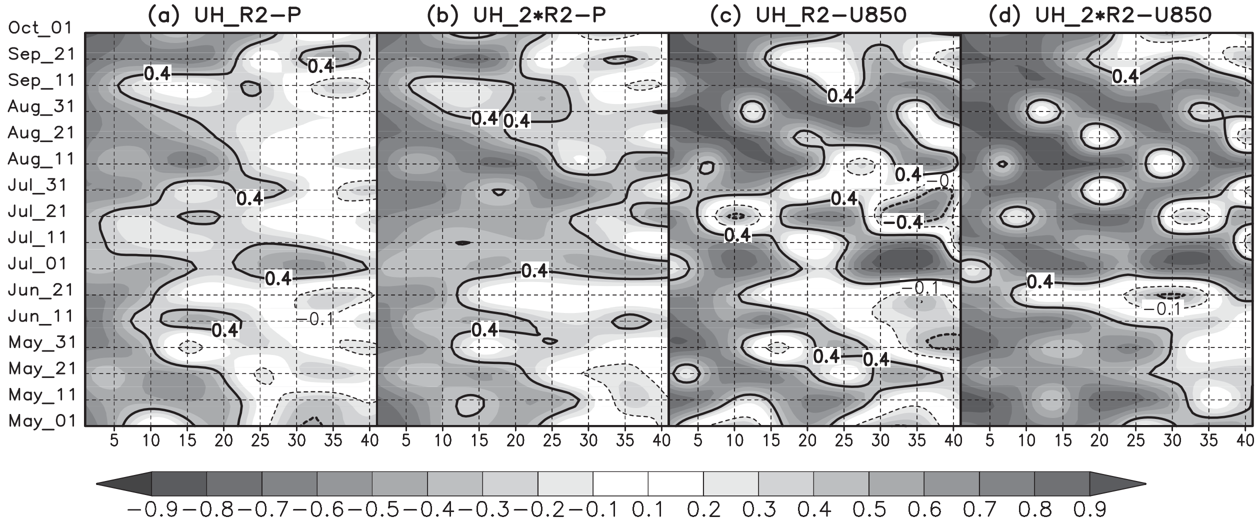

FIG. 11. As in Fig. 10, but over Southeast Asia.

In addition to the 2004 summer (Fu et al. 2009) and the 2008 summer, will recovered ISO signals in initial conditions extend its prediction skills for other years? Figure 12 gives the ISO prediction skills over Southeast Asia in continuous 5 yr (2004–08) initialized with the nudged NCEP-R2, spatially smoothed NCEP-R2[3] and with signal-recovered NCEP-R2 and ERA-Interim along with the CFS forecasts in the 2008 summer. Overall, the forecasts initialized with spatially smoothed NCEP-R2 have the lowest prediction skills. This result suggests that small-scale synoptic disturbances in initial conditions generally act to extend ISO prediction. Future in-depth study is needed to reveal the underlying physical processes. The forecasts initialized with signal-recovered reanalysis consistently outperform that initialized with the nudged reanalysis. The skills initialized with signal-recovered NCEP-R2 and ERA-Interim are very similar. In the 2008 summer, initially the skill of U850 in the NCEP-CFS is obviously higher than that in the UH-HCM, but the resultant prediction skills are almost the same. On the other hand, rainfall prediction skill in the NCEP-CFS is much lower than that in the UH-HCM, which is due to the too slow northward propagation of the ISO in the NCEP-CFS (Fig. 9a).

Figure 13 presents 5-yr prediction skills of ISO-related U850 and rainfall over the global tropics. Similar as that over Southeast Asia, the forecasts initialized with signal-recovered NCEP-R2 and ERA-Interim have consistently higher prediction skills than that initialized with the nudged NCEP-R2. In the 2008 summer, the prediction skill of U850 in the NCEP CFS is slightly higher than that in the UH-HCM initialized with the nudged NCEP-R2, but still being consistently shorter than that initialized with signal-recovered NCEP-R2 and ERA-Interim. Although the rainfall prediction skill of the CFS over Southeast Asia is much shorter than that of the UH-HCM (Fig. 12b), the skill of the CFS and the UH-HCM over the global tropics are actually very similar, likely due to both models suffering from prediction barrier over the Maritime Continent.

The 5-yr mean (2004–08) prediction skills of U850 and rainfall initialized with the nudged and signal-recovered reanalyses over the global tropics and Southeast Asia are summarized into Fig. 14. Over the global tropics, the prediction skills of U850 and rainfall are 14 and 7 days when initialized with the nudged NCEP-R2 and increase to 20 and 10 days when initialized with the signal-recovered NCEP-R2 and ERA-Interim. Over Southeast Asia, the forecast skills of U850 and rainfall are 19 and 11 days when initialized with the nudged NCEP-R2 and increase to 23 and 18 days when initialized with the signal-recovered NCEP-R2 and ERA-Interim. These results indicate that signal-recovered reanalysis extends the prediction skills of that initialized with the nudged reanalysis by 3–6 days over the global tropics and 4–7 days over Southeast Asia. It is also noted that the ISO skill measured with OLR is consistently shorter than that measured with rainfall (Figs. 14b,d) in the UH-HCM model.

In addition to the anomaly spatial pattern correlations used in the above, we also measured the intraseasonal prediction skills with the Wheeler–Hendon index as used in Lin et al. (2008) and Gottschalck et al. (2010). Model-forecasted OLR and zonal winds at 850 and 200 hPa have been used to construct the Wheeler–Hendon index.

[3] Variability with horizontal scale smaller than 10° has been filtered out in the original NCEP-R2 reanalysis before nudging into the UH-HCM.

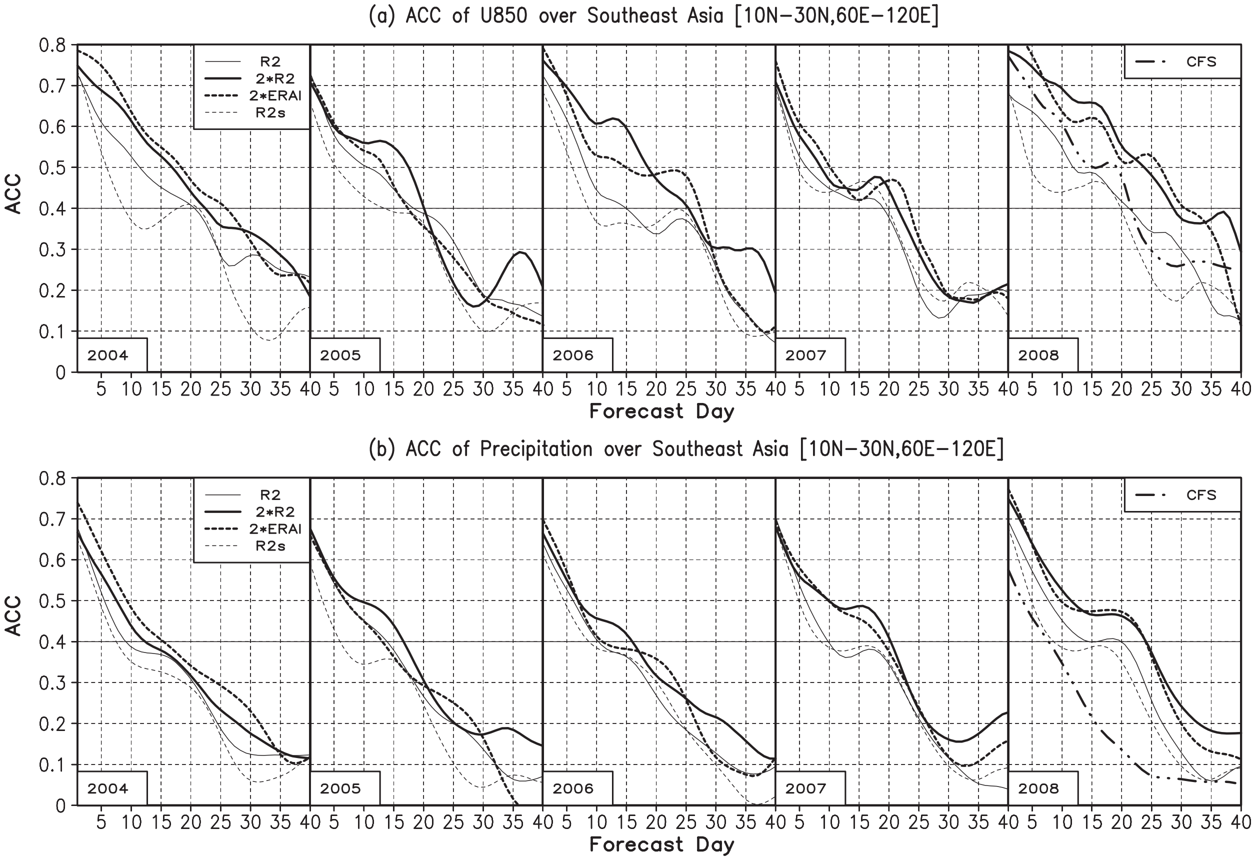

FIG. 12. ACC of (a) U850 and (b) precipitation over Southeast Asia forecasted by the UH-HCM in the 2004–08 summer seasons initialized with the nudged NCEP-R2 (thin gray solid lines), spatially smoothed NCEP-R2 (thin gray dashed lines), signal-recovered NCEP-R2 (black solid lines), and signal-recovered ERA-Interim (black dashed lines). The ACC of NCEP CFS forecasts (dash–dot lines) initialized with the NCEP-R2 was also given for the 2008 summer.

Figure 15 summarizes our results. If the intraseasonal prediction skill is defined as the lead time when ACC drops to 0.5, the skills of the UH-HCM model are 7 and 14 days, respectively, with nudged NCEP-R2 and ERA-Interim as initial conditions. When signal-recovered reanalyses were used as initial conditions, the skills show consistently increases for both the R2 and the ERA-Interim. The skill for the R2 has been doubled to 14 days. The skill increase for the ERA-Interim, however, is only about 1 day. This may suggest that a better signal-recovery method is needed for the ERA-Interim or the skill has matured for our model. Further research is needed to address this issue.

6. Conclusions and prospectus

In this study, we have shown that three reanalysis datasets (NCEP-R1, -R2, and ERA-Interim) underestimated the intensity of equatorial eastward-propagating ISO. When they are directly used to initialize the forecasts, the intraseasonal prediction skills do not reach the optimum, particularly for the R1 and R2. One idea of signal recovery has been proposed to improve the description of the ISO in these reanalyses. At the same time, EDN is introduced to improve initial conditions. When both signal-recovery method and EDN are used to produce initial conditions, the prediction skills of the ISO are consistently extended over the global tropics and Southeast Asia for the recent 5 summers (2004–08). It is also found that including small-scale synoptic disturbances in the initial conditions generally extends the ISO prediction skills (Figs. 12 and 13).

Among the three reanalysis datasets, the NCEP-R2 has the largest ISO variability but lowest spatial correlations with the observations (Fig. 1 and Table 1). Too much small-scale and westward-propagating disturbances exist in the NCEP-R2 (Fig. 2b). Nudging NCEP-R2 to the UH-HCM, in some degree, alleviates these problems. The ERA-Interim has the highest spatial–temporal correlations with the observations (Fig. 2c and Table 1),

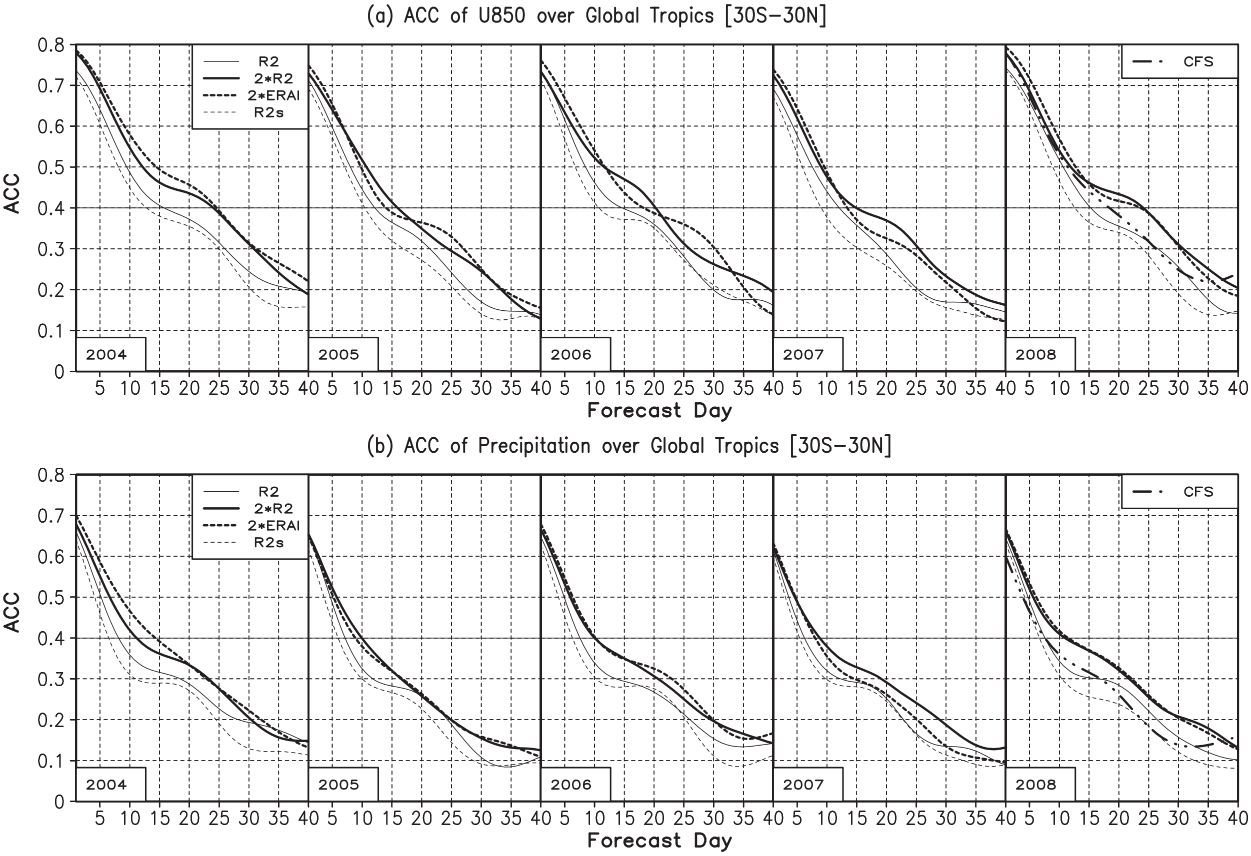

FIG. 13. As in Fig. 12, but over the global tropics.

largely attributing to the assimilation of observed surface rain rate (Andersson et al. 2005). However, the magnitudes of intraseasonal variability in the ERA-Interim are underestimated (Figs. 1 and 2). After doubling the ISO signals in the original reanalyses, then nudging into the UH-HCM, the resultant products (also called signal-recovered reanalyses) have much improved description of the ISO, particularly for the NCEP-R1 and -R2 (Figs. 2e,f and Table 2). For the ERA-Interim, the overall ISO intensity has been increased, but correlations with the observations have dropped. This result suggests that different signal-recovery methods should be explored for different reanalysis datasets.

The impacts of different initial conditions on ISO prediction skills are assessed in this study. Although three reanalyses (NCEP-R1, -R2, ERA-Interim) have different biases, the resultant seasonal-mean ISO forecast skills targeting the 2004 summer are similar (Fig. 5) when default nudging strength in the ECHAM4 model is used. Sensitivity experiments suggested that the default nudging strength of divergence in the ECHAM4 model is too weak, resulting in fictitious rainfall over the equatorial Indian Ocean (Fig. 4). After increasing the divergence nudging strength to the value used in Jeuken et al. (1996), the nudged initial conditions are consistently better than that using default divergence nudging (Figs. 3 and 4), as are the ISO prediction skills (Fig. 5). The resultant extension of the intraseasonal U850's prediction skill reaches 10 days over Southeast Asia. In this case, the skills using ERA-Interim as initial conditions are consistently higher than that using NCEP-R1 and -R2 except for rainfall over Southeast Asia (Fig. 5).

Preliminary analysis suggests that both the UH-HCM and NCEP CFS suffer prediction barrier over the Maritime Continent. The forecasts with initial ISO-related convection over the Maritime Continent have the lowest skills. The highest skills usually appear after initial convection moves to the east of the Maritime Continent. The ISO prediction skills of the UH-HCM and NCEP CFS in the 2008 summer [i.e., the target year of YOTC and the Asian Monsoon Year (AMY; 2007–12); the details of AMY can be found online at http://www.wcrp–amy.org/] have been compared (Figs. 7 and 8). It is found that the UH-HCM has much better rainfall prediction skill over Southeast Asia than the CFS (Figs. 8 and 12b), because the northward-propagating ISO is too

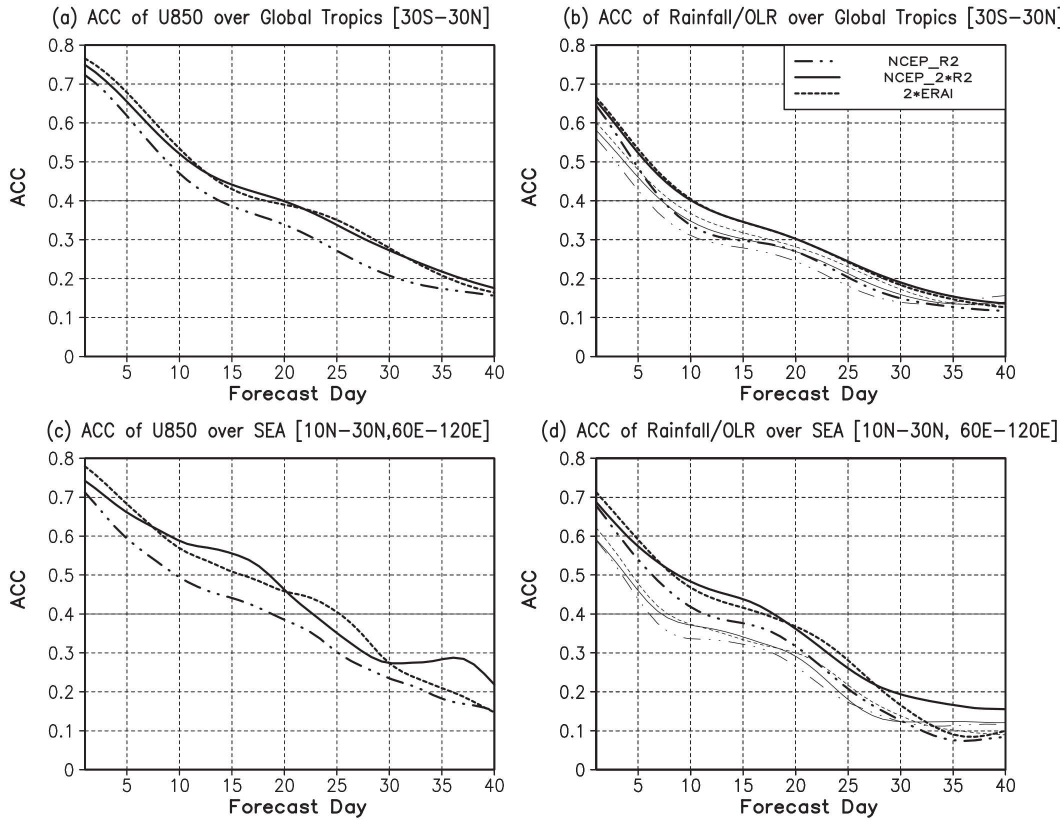

FIG. 14. The 5-yr (2004–08) mean ACC of UH-HCM forecasts initialized with the nudged NCEP-R2 (dash–dot lines), signal-recovered NCEP-R2 (solid lines), and signal-recovered ERA-Interim (dash lines): (a) for U850 over the global tropics, (b) for rainfall (thick lines)/OLR (thin lines) over the global tropics, (c) for U850 over Southeast Asia, and (d) for rainfall (thick lines) /OLR (thin lines) over Southeast Asia.

slow in the CFS[4] (Fig. 9; also see W. Q. Wang et al. 2009; Achuthavarier and Krishnamurthy 2009). Over the global tropics, both the UH-HCM and NCEP-CFS have similar prediction skills (Fig. 13) and suffer prediction barrier over the Maritime Continent.

The forecasts initialized with signal-recovered reanalyses have consistently higher skills than that initialized with the nudged reanalyses in a continuous 5-yr period (2004–08; Figs. 12, 13, 14, and 15). With the EDN introduced in this study, 5 summer-mean prediction skills of U850 and rainfall over Southeast Asia reaches 19 and 11 days even when initialized with the nudged NCEP-R2. When initialized with signal-recovered NCEP-R2 and ERA-Interim, prediction skills extend to 23 and 18 days for U850 and rainfall. The corresponding skills for global tropics are relatively shorter, which are 14 and 7 days when initialized with the nudged NCEP-R2 and increase to 20 and 10 days when initialized with signal-recovered NCEP-R2 and ERA-Interim. When measured with the Wheeler–Hendon index, the intraseasonal prediction skills are 7 and 14 days, respectively, for the nudged and signal-recovered R2. The skills are 14 and 15 days for the nudged and signal-recovered ERA-Interim (Fig. 15).

The present results demonstrated that by taking advantage of a model with relatively high-quality simulations of the ISO (Fu and Wang 2004) and initialized with the nudged ERA-Interim and signal-recovered R1 and R2, we can achieve useful ISO prediction skills of 2–3 weeks for Southeast Asia and about 2 weeks for the global tropics. Considering the strong modulations of the ISO on tropical cyclones, midlatitude extreme weather, as well as the wet and dry spells of global monsoon systems (e.g., Bessafi and Wheeler 2006; Maloney and Hartmann 2000; Hong et al. 2010; Higgins and Shi 2001; Jones 2000; Yasunari 1979; Annamalai and Slingo 2001; Chen and Weng 1999; Goswami et al. 2003; Sun and Chen 1994, etc.), knowing the phase of the ISO 2–4 weeks ahead offers a reliable source for probabilistic assessments on

[4] Recently, a new version of the CFS has been implemented at NCEP Climate Prediction Center (CPC), which shows improved simulations of the ISO (Weaver et al. 2010). The possible impacts on ISO prediction skills are under assessment at NCEP CPC.

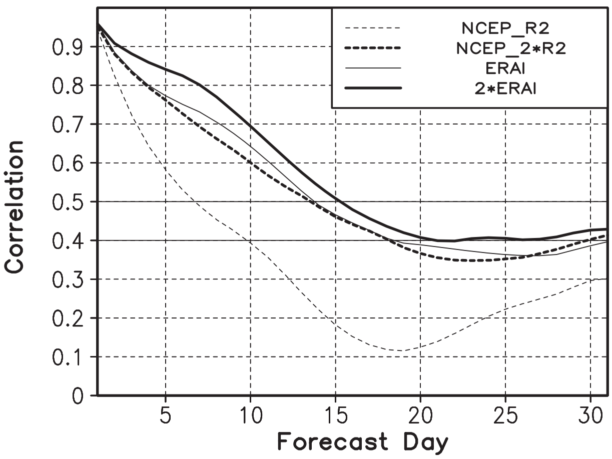

FIG. 15. ACC of the Wheeler–Hendon index as function of forecast lead time. The forecasts were initiated with the nudged NCEP-R2 (gray dashed line), signal-recovered NCEP-R2 (black dashed line), nudged ERA-Interim (gray solid line), and the signal-recovered ERA-Interim (black solid line).

the occurrences of these extreme events (e.g., Gottschalck et al. 2010). This information has great socioeconomic value particularly for those weather-sensitive sectors (e.g., water management, agriculture, disaster prevention, etc.; Wang 2006; Brunet et al. 2010).

The present study is a step toward this direction. To ensure steady progress in the advancement of ISO prediction, synergetic efforts between weather and climate communities are needed at least in three fronts: (i) to improve the representations of multiscale convective systems and their interactions with large-scale circulations in atmospheric models, which are key processes of the observed ISO; (ii) to advance the coupling processes among atmosphere, ocean, and land that are crucial to the realistic simulations of the ISO; and (iii) to acquire better initial conditions, through deploying new observations and developing new data assimilation techniques, for the atmosphere–ocean–land coupled forecast systems.

Recently, great efforts have been made at the National Oceanic and Atmospheric Administration (NOAA) NCEP and the National Aeronautics and Space Administration (NASA) Goddard Space Flight Center (GSFC) to produce two new reanalysis datasets: Climate Forecast System Reanalysis (CFSR) and the Modern Era Retrospective Analysis for Research and Applications (MERRA; Saha et al. 2010; Bosilovich 2008; Rienecker et al. 2009). It is expected that the CFSR and MERRA have better quality than the NCEP-R1 and -R2 in describing tropical weather and climate variability. Future studies will be conducted to evaluate the ISO in the CFSR and MERRA and to assess the ISO prediction skills when the CFSR and MERRA are used as initial conditions.

Acknowledgments. This work was sponsored by the Japan Agency for Marine-Earth Science and Technology (JAMSTEC), NASA, and NOAA through their support of the IPRC. Additional support comes from NOAA, DOE, NSF, and the APEC Climate Center (APCC) as part of the APCC International Research Project (CLiPAS) and the Korean Meteorological Administration Research and Development Program (RACS 2010-2017). We thank Dr. Hai Lin at Environment Canada for sharing his codes to calculate MJO skill.

REFERENCES

Achuthavarier, D., and V. Krishnamurthy, 2009: Daily modes of South Asian summer monsoon variability in the NCEP Climate Forecast System. COLA Tech. Rep. 287, 43 pp. [Available online at ftp://grads.iges.org/pub/ctr/CTR287_ms.pdf.]

Andersson, E., and Coauthors, 2005: Assimilation and modeling of the atmospheric hydrological cycle in the ECMWF forecasting system. *Bull. Amer. Meteor. Soc.,* **86,** 387–402.

Annamalai, H., and J. M. Slingo, 2001: Active/break cycles: Diagnosis of the intraseasonal variability of the Asian summer monsoon. *Climate Dyn.,* **18,** 85–102.

Bechtold, P., M. Kohler, T. Jung, F. Doblas-Reyes, M. Leutbecher, M. J. Rodwell, F. Vitart, and G. Balsamo, 2008: Advances in simulating atmospheric variability with the ECMWF model: From synoptic to decadal time-scales. *Quart. J. Roy. Meteor. Soc.,* **134,** 1337–1351.

Bessafi, M., and M. C. Wheeler, 2006: Modulation of south Indian Ocean tropical cyclones by the Madden–Julian Oscillation and convectively coupled equatorial waves. *Mon. Wea. Rev.,* **134,** 638–656.

Bosilovich, M., 2008: NASA's Modern Era Retrospective-analysis for research and applications: Integrating earth observations. *Earthzine*. [Available online at http://www.earthzine.org/2008/09/26/nasas-modern-era-retrospective-analysis/.]

Brunet, G., and Coauthors, 2010: Collaboration of the weather and climate communities to advance subseasonal-to-seasonal prediction. *Bull. Amer. Meteor. Soc.,* **91,** 1397–1406.

Chen, T. C., and J. C. Alpert, 1990: Systematic errors in the annual and intraseasonal variations of the planetary-scale divergent circulation in NMC medium-range forecasts. *Mon. Wea. Rev.,* **118,** 2607–2623.

——, and S.-P. Weng, 1999: Interannual and intraseasonal variations in monsoon depressions and their westward-propagating predecessors. *Mon. Wea. Rev.,* **127,** 1005–1020.

Fu, X., and B. Wang, 2001: A coupled modeling study of the annual cycle of Pacific cold tongue. Part I: Simulation and sensitivity experiments. *J. Climate,* **14,** 765–779.

——, and ——, 2004: The boreal-summer intraseasonal oscillations simulated in a hybrid coupled atmosphere–ocean model. *Mon. Wea. Rev.,* **132,** 2628–2649.

——, ——, T. Li, and J. P. McCreary, 2003: Coupling between northward-propagating intraseasonal oscillations and sea surface temperature in the Indian Ocean. *J. Atmos. Sci.,* **60,** 1733–1753.

——, ——, and L. Tao, 2006: Satellite data reveal the 3-D moisture structure of Tropical Intraseasonal Oscillation and its coupling with underlying ocean. *Geophys. Res. Lett.,* **33,** L03705, doi:10.1029/2005GL025074.

——, ——, D. E. Waliser, and L. Tao, 2007: Impact of atmosphere-ocean coupling on the predictability of monsoon intraseasonal oscillations. *J. Atmos. Sci.,* **64,** 157–174.

——, B. Yang, Q. Bao, and B. Wang, 2008a: Sea surface temperature feedback extends the predictability of tropical intraseasonal oscillation. *Mon. Wea. Rev.,* **136,** 577–597.

——, B. Wang, Q. Bao, P. Liu, and B. Yang, 2008b: Experimental dynamical forecast of an MJO event observed during TOGA-COARE period. *Atmos. Oceanic Sci. Lett.,* **1,** 24–28.

——, ——, ——, ——, and J.-Y. Lee, 2009: Impacts of initial conditions on monsoon intraseasonal forecasting. *Geophys. Res. Lett.,* **36,** L08801, doi:10.1029/2009GL037166.

Gottschalck, J., and Coauthors, 2010: A framework for assessing operational Madden–Julian oscillation forecasts: A CLIVAR MJO working group project. *Bull. Amer. Meteor. Soc.,* **91,** 1247–1258.

Hendon, H. H., B. Liebmann, M. Newmann, J. D. Glick, and J. E. Schemm, 2000: Medium-range forecast errors associated with active episodes of the Madden–Julian oscillation. *Mon. Wea. Rev.,* **128,** 69–86.

Higgins, W., and W. Shi, 2001: Intercomparison of the principle modes of interannual and intraseasonal variability of the North American monsoon system. *J. Climate,* **14,** 403–417.

Hong, C.-C., M.-Y. Lee, H.-H. Hsu, and J.-L. Kuo, 2010: Role of submonthly disturbance and 40-50-day ISO on the extreme rainfall event associated with Typhoon Morakot (2009) in Southern Taiwan. *Geophys. Res. Lett.,* **37,** L08805, doi:10.1029/2010GL042761.

Hurrell, J., G. A. Meehl, D. Bader, T. L. Delworth, B. Kirtman, and B. Wielicki, 2009: A unified modeling approach to climate system prediction. *Bull. Amer. Meteor. Soc.,* **90,** 1819–1832.

Jeuken, A. B. M., P. C. Siegmund, L. C. Heijboer, J. Feichter, and L. Bengtsson, 1996: On the potential of assimilating meteorological analyses in a global climate model for the purpose of model validation. *J. Geophys. Res.,* **101** (D12), 16 939–16 950.

Jiang, X. A., D. E. Waliser, M. C. Wheeler, C. Jones, M. I. Lee, and S. D. Schubert, 2008: Assessing the skill of an all-season statistical forecast model for the Madden–Julian oscillation. *Mon. Wea. Rev.,* **136,** 1940–1956.

Jones, C., 2000: Occurrence of extreme precipitation events in California and relationships with the Madden–Julian oscillation. *J. Climate,* **13,** 3576–3587.

——, D. E. Waliser, J.-K. E. Schemm, and W.K.-M. Lau, 2000: Prediction skill of the Madden–Julian Oscillation in dynamical extended range forecasts. *Climate Dyn.,* **16,** 273–289.

——, L. M. V. Carvalho, R. W. Higgins, D. E. Waliser, and J.-K. E. Schemm, 2004: A statistical forecast model of tropical intraseasonal convective anomalies. *J. Climate,* **17,** 2078–2095.

Kalnay, E., and Coauthors, 1996: The NCEP/NCAR 40-Year Reanalysis Project. *Bull. Amer. Meteor. Soc.,* **77,** 437–471.

Kanamitsu, M., W. Ebisuzaki, J. Woollen, S.-K. Yang, J. J. Hnilo, M. Fiorino, and G. L. Potter, 2002: NCEP-DEO AMIP-II Reanalysis (R-2). *Bull. Amer. Meteor. Soc.,* **83,** 1631–1643.

Kang, I.-S., and H.-H. Kim, 2010: Assessment of MJO predictability for boreal winter with various statistical and dynamical models. *J. Climate,* **23,** 2368–2378.

Kim, D., and Coauthors, 2009: Application of MJO simulation diagnostics to climate models. *J. Climate,* **22,** 6413–6436.

Kim, H. M., C. D. Hoyos, P. J. Webster, and I. S. Kang, 2008: Sensitivity of MJO simulation and predictability to sea surface temperature variability. *J. Climate,* **21,** 5304–5317.

Kistler, R., and Coauthors, 2001: The NCEP–NCAR 50-Year Reanalysis: Monthly means CD-ROM and documentation. *Bull. Amer. Meteor. Soc.,* **82,** 247–267.

Klingaman, N. P., P. M. Inness, H. Weller, and J. M. Slingo, 2008: The importance of high-frequency sea-surface temperature variability to the intraseasonal oscillation of Indian monsoon rainfall. *J. Climate,* **21,** 6119–6140.

Koster, R. D., M. J. Suarez, and M. Heiser, 2000: Variance and predictability at seasonal-to-interannual timescales. *J. Hydrometeor.,* **1,** 26–46.

Krishnamurti, T. N., M. Subramaniam, G. Daughenbaugh, D. Oosterhof, and J. H. Xue, 1992: One-month forecast of wet and dry spells of the monsoon. *Mon. Wea. Rev.,* **120,** 1191–1223.

Lau, K. M., and F. C. Chang, 1992: Tropical intraseasonal oscillation and its prediction by the NMC operational model. *J. Climate,* **5,** 1365–1378.

Lin, H., G. Brunet, and J. Derome, 2008: Forecast skill of the Madden–Julian oscillation in two Canadian atmospheric models. *Mon. Wea. Rev.,* **136,** 4130–4149.

Lin, J. L., and Coauthors, 2006: Tropical intraseasonal variability in 14 IPCC AR4 climate model. Part I: Convective signals. *J. Climate,* **19,** 2665–2690.

Lorenz, E. N., 1963: Deterministic nonperiodic flow. *J. Atmos. Sci.,* **20,** 130–141.

——, 1993: *The Essence of Chaos*. University of Washington Press, 227 pp.

Madden, R. A., and P. R. Julian, 1972: Description of global-scale circulation cells in the tropics with a 40-50 day period. *J. Atmos. Sci.,* **29,** 1109–1123.

Maloney, E. D., and D. L. Hartmann, 2000: Modulation of eastern North Pacific hurricanes by the Madden–Julian Oscillation. *J. Climate,* **13,** 1451–1460.

Mitovski, T., I. Folkins, K. von Salzen, and M. Sigmond, 2010: Temperature, relative humidity, and divergence response to high rainfall events in the tropics: Observations and models. *J. Climate,* **23,** 3613–3625.

Moncrieff, M. W., M. A. Shapiro, J. M. Slingo, and F. Molteni, 2007: Collaborative research at the intersection of weather and climate. *WMO Bull.,* **56,** 204–211.

Newman, M., P. D. Sardeshmukh, C. R. Winkler, and J. S. Whitaker, 2003: A study of subseasonal predictability. *Mon. Wea. Rev.,* **131,** 1715–1732.

Nobre, C., G. P. Brasseur, M. A. Shapiro, M. Lahsen, G. Brunet, A. J. Busalacchi, K. Hibbard, and K. Noone, 2010: Addressing the complexity of the Earth system. *Bull. Amer. Meteor. Soc.,* **91,** 1389–1396.

Nordeng, T. E., 1995: Extended version of the convective parameterization scheme at ECMWF and their impact on the mean and transient activity of the model in the tropics. ECMWF Research Department Tech. Memo. 206, European Centre for Medium-Range Weather Forecasts, Reading, United Kingdom, 41 pp.

Palmer, T. N., F. J. Doblas-Reyes, A. Weisheimer, and M. J. Rodwell, 2008: Toward seamless prediction: Calibration of climate change projections using seasonal forecasts. *Bull. Amer. Meteor. Soc.,* **89,** 459–470.

Pegion, K., and B. P. Kirtman, 2008: The impact of air–sea interactions on the simulation of tropical intraseasonal variability. *J. Climate,* **21,** 6616–6635.

Reichler, T., and J. O. Roads, 2005: Long-range predictability in the tropics. Part II: 30–60-day variability. *J. Climate,* **18,** 634–650.

Rienecker, M., and Coauthors, cited 2009: MERRA—NASA's reanalysis overview of the system. NASA GSFC, Global Modeling and Assimilation Office. [Available online at http://gmao.gsfc.nasa.gov/pubs/docs/Rienecker377.pdf.]

Roeckner, E., and Coauthors, 1996: The atmospheric general circulation model ECHAM-4: Model description and simulation of present-day climate. Max-Planck-Institute for Meteorology Rep. 218, 90 pp.

Saha, S., and Coauthors, 2006: The NCEP Climate Forecast System. *J. Climate,* **19,** 3483–3517.

——, and Coauthors, 2010: The NCEP Climate Forecast System reanalysis. *Bull. Amer. Meteor. Soc.,* **91,** 1015–1057.

Seo, K.-H., J.-K. E. Schemm, C. Jones, and S. Moorthi, 2005: Forecast skill of the tropical intraseasonal oscillation in the NCEP GFS dynamical extended range forecasts. *Climate Dyn.,* **25,** 265–284.

——, W.-Q. Wang, J. Gottschalck, Q. Zhang, J.-K. E. Schemm, W. R. Higgins, and A. Kumar, 2009: Evaluation of MJO forecast skill from several statistical and dynamical forecast models. *J. Climate,* **22,** 2372–2388.

Shapiro, M. A., and Coauthors, 2010: An Earth-system prediction initiative for the twenty-first century. *Bull. Amer. Meteor. Soc.,* **91,** 1377–1388.

Shinoda, T., H. H. Hendon, and J. Glick, 1999: Intraseasonal surface fluxes in the tropical western Pacific and Indian Oceans from NCEP reanalysis. *Mon. Wea. Rev.,* **127,** 678–693.

Shukla, J., 1981: Dynamical predictability of monthly means. *J. Atmos. Sci.,* **38,** 2547–2572.

——, 1998: Predictability in the midst of chaos: A scientific basis for climate forecasting. *Science,* **282,** 728–731.

——, R. Hagedorn, B. Hoskins, J. Kinter, J. Marotzke, M. Miller, T. N. Palmer, and J. Slingo, 2009: Strategies—Revolution in climate prediction: A declaration at the world modeling summit for climate prediction. *Bull. Amer. Meteor. Soc.,* **90,** 175–178.

Simmons, A., S. Uppala, D. Dee, and S. Kobayashi, 2007: ERA-Interim: New ECMWF reanalysis products from 1989 onwards. *ECMWF Newsletter,* No. 110, ECMWF, Reading, United Kingdom, 25–35. [Available online at http://www.ecmwf.int/publications/newsletters/pdf/110_rev.pdf.]

Slingo, J. M., and Coauthors, 1996: Intraseasonal oscillations in 15 atmospheric general circulation models: Results from an AMIP diagnostic subproject. *Climate Dyn.,* **12,** 325–357.

Sperber, K. R., and H. Annamalai, 2008: Coupled model simulations of boreal-summer intraseasonal (30-50-day) variability. Part I: Systematic errors and caution on use of metrics. *Climate Dyn.,* **31,** 345–372.

Sun, G. W., and B. D. Chen, 1994: Clustering of Tibetan Plateau vortex by atmospheric intraseasonal oscillation. *Sci. Atmos. Sin.,* **18,** 113–121.

Susskind, J., 2007: Improved atmospheric soundings and error estimates from analysis of AIRS/AMSU data. *Atmospheric and Environmental Remote Sensing Data Processing and Utilization III: Readiness for GEOSS,* M. D. Goldberg et al., Eds., International Society for Optical Engineering (SPIE Proceedings, Vol. 6684), 66840M-66840M-12, doi:10.1117/12.734336.

Tian, B. J., D. E. Waliser, E. J. Fetzer, B. H. Lambrigtsen, Y. L. Yung, and B. Wang, 2006: Vertical moist thermodynamic structure and spatial-temporal evolution of the MJO in AIRS observations. *J. Atmos. Sci.,* **63,** 2462–2485.

Tiedtke, M., 1989: A comprehensive mass flux scheme for cumulus parameterization in large-scale models. *Mon. Wea. Rev.,* **117,** 1779–1800.

Toth, Z., M. Pena, and A. Vintzileos, 2007: Bridging the gap between weather and climate forecasting: Research priorities for intraseasonal prediction. *Bull. Amer. Meteor. Soc.,* **88,** 1427–1429.

Uppala, S., and Coauthors, 2005: The ERA-40 reanalysis. *Quart. J. Roy. Meteor. Soc.,* **131,** 2961–3012.

——, D. Dee, S. Kobayashi, P. Berrisford, and A. Simmons, 2008: Status update of ERA-Interim. *ECMWF Newsletter,* No. 115, ECMWF, Reading, United Kingdom, 12–18. [Available online at http://www.ecmwf.int/publications/newsletters/pdf/115.pdf.]

Vintzileos, A., and H.-L. Pan, cited 2007: Subseasonal prediction with the NCEP-CFS: Forecast skill and prediction barriers for tropical intraseasonal oscillations. NOAA. [Available online at http://www.cpc.ncep.noaa.gov/products/outreach/proceedings/ cdw32_proceedings/Augustin_Vintzileos.ppt.]

Vitart, F., and F. Molteni, 2009: Dynamical extended-range prediction of early monsoon rainfall over India. *Mon. Wea. Rev.,* **137,** 1480–1492.

——, and Coauthors, 2007: Monthly forecast of the Madden–Julian oscillation using a coupled GCM. *Mon. Wea. Rev.,* **135,** 2700–2715.

——, and Coauthors, 2008: The new VarEPS-monthly forecasting system: A first step towards seamless prediction. *Quart. J. Roy. Meteor. Soc.,* **134,** 1789–1799.

Waliser, D. E., C. Jones, J.-K. E. Schemm, and N. E. Graham, 1999: A statistical extended-range tropical forecast model based on the slow evolution of the Madden–Julian oscillation. *J. Climate,* **12,** 1918–1939.

——, K. M. Lau, W. Stern, and C. Jones, 2003a: Potential predictability of the Madden–Julian oscillation. *Bull. Amer. Meteor. Soc.,* **84,** 33–50.

——, and Coauthors, 2003b: AGCM simulations of intraseasonal variability associated with the Asian Summer Monsoon. *Climate Dyn.,* **21,** 423–446.

——, and Coauthors, 2006: The experimental MJO prediction project. *Bull. Amer. Meteor. Soc.,* **87,** 425–431.

——, and Coauthors, cited 2009: Year of Tropical Convection (YOTC) science plan. [Available online at http://www.ucar.edu/yotc/index.html.]

Wang, B., 2006: *The Asian Monsoon*. Springer and Praxis Publishing, 787 pp.

——, and H. Rui, 1990: Synoptic climatology of transient tropical intraseasonal convection anomalies: 1975-1985. *Meteor. Atmos. Phys.,* **44,** 43–61.

——, T. Li, and P. Chang, 1995: An intermediate model of the tropical Pacific Ocean. *J. Phys. Oceanogr.,* **25,** 1599–1616.

——, and Coauthors, 2009: Advance and prospectus of seasonal prediction: Assessment of the APCC/CLiPAS 14-model ensemble retrospective seasonal prediction (1980–2004). *Climate Dyn.,* **33,** 93–117, doi:10.1007/S00382-008-0460-0.

Wang, W. Q., M. Y. Chen, and A. Kumar, 2009: Impacts of ocean surface on the northward propagation of the boreal-summer intraseasonal oscillation in the NCEP climate forecast system. *J. Climate,* **22,** 6561–6576.

Weaver, S., W. Wang, and A. Kumar, 2010: Representation of MJO variability in the NCEP Climate Forecast System. Preprints, *22nd Conf. on Climate Variability and Change,* Atlanta, GA, Amer. Meteor. Soc., 4A.2. [Available online at http://ams.confex.com/ams/90annual/techprogram/paper_161235.htm.]

Weng, F. Z., T. Zhu, and B. H. Yan, 2007: Satellite data assimilation in numerical weather prediction models. Part II: Uses of rain-affected radiances from microwave observations for hurricane vortex analysis. *J. Atmos. Sci.,* **64,** 3910–3925.

Wheeler, M. C., and H. H. Hendon, 2004: An all-season real-time multivariate MJO index: Development of an index for monitoring and prediction. *Mon. Wea. Rev.,* **132,** 1917–1932.

Wilks, D. S., 2005: *Statistical Methods in the Atmospheric Sciences*. 2nd ed. Elsevier, 627 pp.

Woolnough, S. J., F. Vitart, and M. A. Balmaseda, 2007: The role of the ocean in the Madden-Julian Oscillation: Implications for the MJO prediction. *Quart. J. Roy. Meteor. Soc.,* **133,** 117–128.

Yasunari, T., 1979: Cloudiness fluctuations associated with the Northern Hemisphere summer monsoon. *J. Meteor. Soc. Japan,* **57,** 227–242.

Zagar, N., E. Andersson, and M. Fisher, 2005: Balanced tropical data assimilation based on a study of equatorial waves in ECMWF short-range forecast errors. *Quart. J. Roy. Meteor. Soc.,* **131,** 987–1011.